Bone microstructure and the evolution of growth patterns in Permo-Triassic therocephalians (Amniota, Therapsida) of South Africa

PeerJ Reviewing Manuscript

The diversity of therocephalian therapsids during the end-Permian mass extinction offers the potential to investigate the evolution of growth patterns across the clade and their underlying influences on post-extinction body size reductions, or 'Lilliput effects.' We present a phylogenetic survey of limb bone histology and growth patterns of therocephalians from the Middle Permian through Middle Triassic of the Karoo Basin, South Africa. Histologic sections were prepared from 80 limb bones representing 11 genera of therocephalians. Histologic indicators of skeletal growth, including cortical vascularity (%CV) and mean primary osteon diameters (POD), were evaluated in a phylogenetic framework and assessed for correlations with other biologically significant variables (e.g., size and robusticity). Changes in %CV and POD correlated strongly with evolutionary changes in body size (i.e., smaller-bodied descendants tended to have lower %CV than their larger-bodied ancestors across the tree). Bone wall thickness tended to be high in early therocephalians and lower in the gracile-limbed baurioids, but showed no general correlation with cross-sectional area or degree of vascularity (and, thus, growth). Clade-level patterns, however, deviated from previously studied within-lineage patterns. For example, *Moschorhinus*, one of few therapsid genera to have survived the extinction boundary, demonstrated higher %CV in the Triassic than in the Permian despite its smaller size in the extinction aftermath. Results support a synergistic model of size reductions for Triassic therocephalians, influenced both by within-lineage heterochronic shifts in survivor taxa (as in *Moschorhinus* and the dicynodont *Lystrosaurus*) and cladistically inferred survival of small-bodied taxa that had evolved short growth durations (e.g., baurioids). These findings mirror the multi-causal Lilliput patterns described in marine faunas, but contrast with skeletochronologic studies that suggest slow, prolonged shell secretion over several years in marine benthos. New histologic data and phylogenetic comparative methods will continue to improve our understanding of the evolutionary

dynamics of growth and body size shifts during mass extinctions and recoveries.

PeerJ Reviewing Manuscript

Bone microstructure and the evolution of growth patterns in Permo-Triassic therocephalians (Amniota, Therapsida) of South Africa

Adam K. Huttenlocker*

Department of Biology and Burke Museum of Natural History and Culture, University of Washington, Seattle, Washington 98195, U.S.A. Email: ahuttenlocker@gmail.com;

and

Jennifer Botha-Brink

Department of Karoo Palaeontology, National Museum and Department of Zoology and Entomology, University of the Free State, Bloemfontein 9300, South Africa; Centre of Excellence in Palaeosciences, University of Witwatersrand, Johannesburg 2050, South Africa. Email: jbotha@nasmus.co.za.

*Corresponding author; Current address: Natural History Museum of Utah and Department of Biology, University of Utah, Salt Lake City, Utah, USA 84112-0840

75 pages, 1 appendix, 2 tables, 14 figures

PeerJ Reviewing Manuscript

PeerJ Reviewing Manuscript

Abstract—The diversity of therocephalian therapsids during the end-Permian mass extinction offers the potential to investigate the evolution of growth patterns across the clade and their underlying influences on post-extinction body size reductions, or 'Lilliput effects.' We present a phylogenetic survey of limb bone histology and growth patterns of therocephalians from the Middle Permian through Middle Triassic of the Karoo Basin, South Africa. Histologic sections were prepared from 80 limb bones representing 11 genera of therocephalians. Histologic indicators of skeletal growth, including cortical vascularity (%CV) and mean primary osteon diameters (POD), were evaluated in a phylogenetic framework and assessed for correlations with other biologically significant variables (e.g., size and robusticity). Changes in %CV and POD correlated strongly with evolutionary changes in body size (i.e., smaller-bodied descendants tended to have lower %CV than their larger-bodied ancestors across the tree). Bone wall thickness tended to be high in early therocephalians and lower in the gracile-limbed baurioids, but showed no general correlation with cross-sectional area or degree of vascularity (and, thus, growth). Clade-level patterns, however, deviated from previously studied within-lineage patterns. For example, *Moschorhinus*, one of few therapsid genera to have survived the extinction boundary, demonstrated higher %CV in the Triassic than in the Permian despite its smaller size in the extinction aftermath. Results support a synergistic model of size reductions for Triassic therocephalians, influenced both by within-lineage heterochronic shifts in survivor taxa (as in *Moschorhinus* and the dicynodont *Lystrosaurus*) and cladistically inferred survival of small-bodied taxa that had evolved short growth durations (e.g., baurioids). These findings mirror the multi-causal Lilliput patterns described in marine faunas, but contrast with skeletochronologic studies that suggest slow, prolonged shell secretion over several years in marine benthos. New histologic data and phylogenetic comparative methods will continue to

improve our understanding of the evolutionary dynamics of growth and body size shifts during mass extinctions and recoveries.

Introduction

Mass extinctions are frequently followed by short-term reductions in body sizes of survivor lineages, a pattern known as the 'Lilliput effect' (Urbanek, 1993; Harries, Kauffman & Hansen, 1996). However, in the absence of adequate phylogenetic and life history data, the mechanisms of size reductions can be unclear and may differ across environments, taxonomic groups, and extinction events (Twitchett, 2007; Harries and Knorr, 2009). Lilliput patterns have been documented widely in marine invertebrate groups following the end-Permian extinction (Payne, 2005; Twitchett, 2007; Luo et al., 2008; Mutter and Neuman, 2009; Metcalfe, Twitchett & Price-Lloyd, 2011; Song, Tong & Chen, 2011; Rego et al., 2012), and anecdotally in tetrapods of the Triassic *Lystrosaurus* Assemblage Zone in the Karoo Basin of South Africa (ca. 252.3 Ma), but growth dynamics underlying these patterns are not fully understood. Therocephalians represent an exemplary clade of nonmammalian therapsids that thrived from the Middle Permian to Middle Triassic, and survived the end-Permian extinction as important components of Triassic survivor and recovery faunas in the Karoo Basin (Botha and Smith, 2006). In addition to the dicynodont *Lystrosaurus*, at least three genera of therocephalians in two major groups have observed stratigraphic occurrences that span the extinction boundary in the Karoo: the baurioid *Tetracynodon*, and the akidnognathids *Promoschorhynchus* and *Moschorhinus* (Smith and Botha, 2005; Botha and Smith, 2006; Huttenlocker, Sidor & Smith, 2011). Other Triassic taxa (e.g., *Olivierosuchus*, *Regisaurus*) have long ghost lineages extending into the Permian, indicating that they too survived the extinction but lack a Permian record within the depositional

PeerJ Reviewing Manuscript

basin (Huttenlocker, 2009; Huttenlocker, Sidor & Smith, 2011). Although therocephalians are generally exceeded in abundance by dicynodont therapsids in the Karoo Basin, their diversity, extensive stratigraphic range, and success during the end-Permian extinction make them an ideal group to study evolutionary patterns during the Permian-Triassic transition.

Previous morphological studies of therocephalians have emphasized their functional anatomy, including streptostylic jaw structure and locomotory specializations (e.g., Kemp, 1972, 1978, 1986; Fourie and Rubidge, 2007, 2009). Recent collaborative work on therocephalians has emphasized integration of their fine structure and internal anatomy to resolve paleobiological questions, including tooth replacement patterns, braincase structure, and growth and histomorphologic structure (Abdala, Rubidge & van den Heever, 2008; Sigurdsen et al., 2012; Huttenlocker and Botha-Brink, 2013). Detailed investigations of histmorphology are particularly useful, permitting assessments of growth patterns and variation within or among closely related therapsid species (e.g., Botha and Angielczyk, 2007; Huttenlocker and Botha-Brink, 2013). Moreover, as growth patterns are associated with organismal fitness, recent investigations into bone microstructure have inquired into whether certain growth strategies conferred success on some groups during the end-Permian mass extinction (e.g., rapid growth in the dicynodont *Lystrosaurus*; Botha-Brink and Angielczyk, 2010).

Bone Microstructure in Therapsids

Bone histology has offered insights into the lifestyles and growth patterns of many of the major subclades of nonmammalian therapsids. Recent examples include investigations of feeding and locomotory mechanics, habitat use, and especially growth dynamics (e.g., Ray, Chinsamy & Bandyopadhyay, 2005; Jasinoski, Rayfield & Chinsamy, 2010; Chinsamy-Turan, 2012). Earlier surveys of bone histology emphasized differences between basal (pelycosaurian-grade) synapsid

PeerJ Reviewing Manuscript

PeerJ Reviewing Manuscript

and therapsid tissue composition, matrix organization, and degree of vasculature of the limb bones (Enlow and Brown, 1957; Enlow, 1969; Ricqlès, 1969, 1974a, 1974b, 1976). Particularly, fibrolamellar tissue complexes were found to be near ubiquitous among limb elements of sampled therapsids, suggesting to workers that this tissue complex appeared early during therapsid evolution (Ray, Botha & Chinsamy, 2004; Chinsamy and Hurum, 2006; Ray, Bandyopadhyay & Bhawal, 2009). Indeed, fibrolamellar bone has been reported in basal therapsids (e.g., *Biarmosuchus*: Ricqlès,1974b), as well as in some immature pelycosaurian-grade synapsids (e.g., *Sphenacodon* juveniles) and in fast-growing portions of the skeleton of other basal synapsids (e.g., the elongated neural spines of *Dimetrodon* and crossbars on the neural spines of *Edaphosaurus*) (Huttenlocker, Rega & Sumida, 2010; Huttenlocker, Mazierski & Reisz, 2011; Huttenlocker and Rega, 2012). However, there is great histovariability in the organization of fibrolamellar bone even within major subclades of therapsids. Fibrolamellar bone may be formed by varying degrees of woven- and parallel-fibered interstitial matrix and incorporates a variety of vascular motifs, and may be zonal (punctuated by cyclic growth marks) or azonal. Ray, Botha & Chinsamy (2004) reported the presence of zonal fibrolamellar bone in many Permian and Middle Triassic taxa, but suggested that sustained (non-cyclic) growth patterns might have arisen occasionally in a number of phylogenetically disparate taxa (gorgonopsian *Aelurognathus*; eucynodont *Cynognathus*; and some bidentalian dicynodonts). The abundance of dicynodont fossils in Permian and Triassic rocks and recent advances in their systematic relationships have permitted comparisons of growth patterns in this diverse subclade (Chinsamy and Rubidge, 1993; Botha, 2003; Ray and Chinsamy, 2004; Ray, Chinsamy & Bandyopadhyay, 2005; Botha and Angielczyk, 2007; Ray, Bandyopadhyay & Bhawal, 2009; Botha-Brink and Angielczyk, 2010; Green, Schweitzer & Lamm, 2010; Nasterlack, Canoville &

PeerJ Reviewing Manuscript

Chinsamy-Turan, 2012; Ray, Botha-Brink & Chinsamy-Turan, 2012). Phylogenetic comparative surveys have revealed patterns of increasing tissue vascularity during the evolutionary history of bidentalian dicynodonts (especially in Triassic forms like *Lystrosaurus*), and determinate growth patterns with peripheral rest lines and systematic cortical remodeling in large kannemeyeriiforms (Botha-Brink and Angielczyk, 2010; Green, Schweitzer & Lamm, 2010; Ray, Botha-Brink & Chinsamy-Turan, 2012).

The diversity of growth patterns in other nonmammalian therapsid groups, as well as their phylogenetic and temporal distributions, is incompletely known. A body of literature on nonmammalian cynodont histology has accrued in recent years (e.g., Ricqlès, 1969; Botha and Chinsamy, 2000, 2004, 2005; Ray, Botha & Chinsamy, 2004; Chinsamy and Abdala, 2008; Botha-Brink, Abdala & Chinsamy-Turan, 2012), but sampling has been more limited in other theriodonts, such as the gorgonopsians and therocephalians (Ray, Botha & Chinsamy, 2004; Chinsamy-Turan and Ray, 2012). Ricqlès (1969) suggested differential rates of growth between a basal therocephalian from the Middle Permian of South Africa and the Late Permian whaitsiid '*Notosollasia'* (=*Theriognathus*). Given the comparatively more vascularized cortical bone in the radius of the whaitsiid (1969: plate IV), Ricqlès suggested that therocephalians might have exhibited accelerated growth rates later in their evolutionary history, paralleling the aforementioned temporal pattern of increasing growth rates in some dicynodonts. More recently, Ray, Botha & Chinsamy (2004) and Chinsamy-Turan and Ray (2012) analyzed additional material from an indeterminate scylacosaurid (erroneously identified as '*Pristerognathus'*) and argued for similar 'flexible' growth patterns in gorgonopsians, basal therocephalians, and most early cynodonts. The authors suggested that more rigorous taxonomic sampling would better substantiate parallel trends toward a loss in developmental plasticity and acceleration of growth

rates as in dicynodonts. Inadequate sampling of Late Permian and Triassic eutherocephalians limits our understanding of evolutionary patterns in therapsid histomorphology and skeletal growth during this important geologic transition.

Present Study

Although eutherocephalians have not been sampled histologically for such comparisons, recent revisions to Permo-Triassic boundary-crossing taxa have necessitated cursory descriptions of eutherocephalian histology for its ontogenetic and paleobiological implications (e.g., *Tetracynodon*: Sigurdsen et al., 2012; *Moschorhinus*: Huttenlocker and Botha-Brink, 2013). During the course of this work, we developed a database of histological data and images with the goal of addressing features of life history evolution in Permian and Triassic eutheriodonts (therocephalians and cynodonts), particularly in the context of the end-Permian extinction. Here, we present a reappraisal of limb bone microstructure in Permian and Triassic therocephalians based on new histologic sampling, and offer a hypothesis of the evolution of their growth patterns. We suggest that therocephalians provide a robust study system for investigating the evolution of growth strategies during the Permian-Triassic transition, and a useful point of comparison and contrast to other groups that lived during this time (e.g., dicynodonts, cynodonts).

Materials and Methods

Specimen Selection and Histological Processing

Specimens were selected based on completeness and availability for histological processing, but a broad sample of the major representatives of South African therocephalians was desired in order to recognize long-term patterns (if present) or clade specific

PeerJ Reviewing Manuscript

PeerJ Reviewing Manuscript

histomorphology. Specimens that were semi-articulated and included diagnostic cranial material were preferred for accuracy of taxonomic identifications. Some specimens were not diagnosable to genus, but were resolved to their respective higher taxon as in the case of five indeterminate scylacosaurids described here. Scylacosaurids are generally difficult to identify unless a complete and accurate antecanine tooth count can be made, and some authors have suggested that the diversity of scylacosaurids is over-split because variations in tooth count may be ontogenetically variable (e.g., Abdala, Rubidge & van den Heever, 2008). The sample therefore included 80 limb elements from 33 individuals in 11 genera: *Lycosuchus*, *Glanosuchus*, *Moschorhinus*, *Olivierosuchus*, *Hofmeyria*, *Mirotenthes*, *Theriognathus*, *Ictidosuchoides*, *Tetracynodon*, *Scaloposaurus*, and *Microgomphodon* (Fig. 1), plus additional scylacosaurid material not diagnosed to genus. Thin-sections were prepared using standard histological techniques modified from Chinsamy and Raath (1992) and Wilson (1994). Limb bone midshafts were sampled cross-sectionally and imaged using Nikon Eclipse 50i and LV100 POL petrographic microscopes with a digital image capture system. Histomorphometric variables (discussed below) were measured using NIS-Elements and NIH ImageJ v. 1.42q software. *Moschorhinus* histomorphology was excluded from present description as it has been discussed elsewhere (Huttenlocker and Botha-Brink, 2013), but data from *Moschorhinus* were included in the quantitative analyses (Table 1).

Bone Tissue Typology: Definitions and Selection of Growth Proxies

Bone tissue texture exhibited marked variation in therocephalians and other therapsids, varying from highly organized and lamellar to disorganized and woven. Only a few recent studies have integrated qualitative and quantitative assessments of tissue texture and vascular proxies of growth in Permo-Triassic therapsids (Botha and Chinsamy 2000, 2004, 2005; Ray and

PeerJ Reviewing Manuscript

Chinsamy 2004; Ray et al., 2004, 2005, 2010; Botha-Brink and Angielczyk 2010; Huttenlocker and Botha-Brink, 2013). Generally, cellular bone forms as osteoblasts become incorporated into the extracelluar (or interstitial) matrix (ECM) forming quiescent osteocytes. The overall bone apposition rate affects the texture of the mineralized ECM, with collagen fibers and crystallites bearing a more lamellar organization under slower growth and a nonlamellar (woven-fibered) texture under faster growth. Parallel-fibered bone (as with lamellar bone) can be identified by its 'streaky' appearance under polarized light, with the predominant fiber orientation being parallel to the surface of the bone and forming a woven-basket texture in most cases. In cases in which birefringent properties have been disrupted by diagenetic processes, it is possible to approximate the relative organization of mineralized fibers with reference to the organization of the lacunocanalicular network within the ECM (Stein and Prondvai, 2013). In contrast to parallel-fibered bone, woven-fibered bone includes large, globular osteocyte lacunae that are usually densely packed within the mineralized ECM. Nonlamellar tissues (parallel- and woven-fibered) may also frequently incorporate large vascular canals that later become infilled with one or two concentric lamellae forming primary osteons (diagnosed by their 'Maltese cross' pattern of birefringence under polarized light). These tunnels form passageways for blood vessels and nerves while also contributing to the structural integrity of the bone by providing added bone mass and helping to blunt microcracks. The result is a fibrolamellar bone complex (herein 'FLB'), in which a disorganized, fibrous or nonlamellar interstitial matrix incorporates an anastomosing network of centripetally lamellated primary osteons. Currey (1987, 2002) defined FLB broadly as a tissue complex formed by parallel- (or woven-) fibered bone with primary osteons (2002: p.18). By contrast, Ricqlès (1974a) originally restricted the term 'fibrolamellar' to tissues formed largely by woven-fibered bone with primary osteons, excluding parallel-fibered

bone from this category. Here, we follow the traditional usage of Ricqlès, but temper this strict definition by noting that parallel- and woven-fibered bone form a continuum that is often ill-defined (and may be present simultaneously in many therapsid bony tissues, even within the same section). Bone cortices formed primarily by lamellar tissue, which forms at relatively slower apposition rates (~1 μm/day or less), do not typically incorporate primary osteons, instead bearing simple vascular canals or being avascular. In lamellar bone, the lacunocanalicular network is ordered, the osteocyte lacunae being small and more lenticular in appearance with the long axis oriented parallel to the surface of the bone. Both tissue complexes can be zonal (periodically interrupted by growth marks) or azonal. Growth marks in zonal bone may be present in the form of lines of arrested growth or 'LAGs' (denoted by an opaque cement line, traceable around the entire cortex, and indicative of a temporary cessation of growth) or annuli (thin bands of dense, annular tissue, usually parallel-fibered or lamellar, deposited during periods of slowed growth).

For quantitative histomorphometric analysis, two vascular proxies of skeletal growth were selected: cortical vascularity and mean primary osteon diameter. These proxies were selected in order to evaluate the extent to which histological correlatives of growth varied across phylogeny, and whether their evolution was tied to body size or other biological factors. Vascular proxies have offered useful indicators of skeletal growth in extant and extinct tetrapods (Castanet et al., 2000; Margerie et al., 2002, 2004; Buffrénil, Houssaye & Böhme, 2007; Cubo et al., 2012), and their utility here allows comparisons with other histological studies of therapsids in which similar measures were used (e.g., Botha-Brink and Angielczyk 2010; Huttenlocker and Botha-Brink, 2013). Notably, ontogenetic variation in growth may introduce a lesser degree of cortical vascularity in adult bones that exhibited decreasing apposition rates prior to death and

PeerJ Reviewing Manuscript

PeerJ Reviewing Manuscript

burial, or may introduce variation in a single cross-section. Nonmammalian therapsids, however, are well suited to relative growth rate estimation based on tissue texture and vascularity, due to their generally thick bone walls (preserving the early record of primary growth) and limited secondary remodeling (Botha-Brink and Angielczyk, 2010). Measurement of cortical vascularity (%*CV*, the relative area of the cortex that is occupied by porous, vascular spaces) follows Lee et al. (2013). Measurements were restricted to the inner two-thirds to three-quarters of the cortex where the bone formed at high, sustained growth rates (Cubo et al., 2012), and were averaged from ten quadrants sampled circularly around each midshaft cross-section. The subsampled quadrants excluded areas of secondary reconstruction and outer regions of simple canals. We also estimated mean primary osteon diameter (*POD*) by measuring in microns the transverse (or minimum) widths of 15 primary osteons visible in the subsampled regions and averaging them across all regions within a given midshaft cross-section.

To examine potential effects of size and robusticity on measured histomorphometric variables, we also estimated two proxies of overall bone robusticity: *K* and relative bone wall thickness (*RBT*). These variables play a frequent role in histological studies of fossil tetrapod bone, as bone robusticity may correspond to habitat preferences or mechanical loading (Wall, 1983; Currey and Alexander, 1985; Currey, 2002; Laurin, Girondot & Loth, 2004; Germain and Laurin, 2005; Kriloff et al., 2008). However, their relationships to size, growth, and vascularity have been underexplored in a comparative framework. Whereas *K* represents the proportional diameter of the medullary region relative to the total diameter of the cross-section (Currey and Alexander, 1985), *RBT* represents a percentage of the average cross-sectional thickness of the bone wall relative to the total diameter of the cross-section (Chinsamy, 1993). These measurements, as well as cross-sectional area at midshaft, were attained using NIH ImageJ, and

were tested for correlations with vascular growth proxies using Pearson's product-moment correlation tests. Histomorphometric data are recorded in Table 1.

Correlation Tests

Pearson's product-moment correlation tests—We performed a series of correlation tests in order to evaluate the extent to which variations in vascular growth proxies were dependent upon size and robusticity, which bear a strong influence on many aspects of organismal biology (Peters, 1983; Calder, 1984; Stearns, 1992). For instance, small-bodied therocephalians might have achieved their increasingly diminutive sizes by having a slower growing, less vascularized skeleton compared to their larger-bodied predecessors. In this scenario, one would expect a correlation between smaller size and slower growth, and between larger size and faster growth across subclades. In extant vertebrates, small-bodied species generally exhibit slower growth rates than larger-bodied groups (Case, 1978), a general feature that has also been identified from histologic data in fossil non-avian dinosaurs (Erickson et al., 2004; Lee, 2007). On the other hand, smaller sizes may have been achieved by shortening the duration of the growth period, in which case no generalized correlations between size and vascular proxies of skeletal growth are necessary. To address these hypotheses, histomorphometric data (%*CV*, *POD*, *RBT*) and midshaft cross-sectional area were recorded for each sectioned limb bone. The data were organized into propodial, epipodial, and pooled subsets to control for the effects of increased variance from pooling limb bones of different types (although the effects appeared to be minimal as all tests ultimately yielded similar results). For each data partition, Pearson's product-moment correlation tests were performed between histomorphometric variables (%*CV*, *POD*, *RBT*) and the natural log of midshaft cross-sectional area. Vascular growth proxies were also tested for correlations with bone robusticity independent

PeerJ Reviewing Manuscript

of size, and with each other to assess whether %*CV* and *POD* provided comparable estimates of vascularization.

Phylogeny-independent contrasts—Independent contrast methods were carried out to control for the effects of phylogenetic non-independence of putative correlations (Felsenstein, 1985; Garland, Bennett & Rezende, 2005). For example, one might find low tissue vascularity in Triassic baurioids due to their generally small sizes, or due to their close relatedness (and, by extension, their inherited phenotypic similarities). We carried out additional correlation tests on an augmented data set using the PDAP:PDTREE module (Midford et al., 2011) in Mesquite version 2.0 (Maddison and Maddison, 2007). This required a tree and branch lengths (adapted from Huttenlocker, in review) pruned to the 11 histologically sampled taxa. First, tip data for each of the 11 taxa were recorded in a NEXUS file, including average *%CV*, *POD*, *RBT* and the natural log of midshaft area of the propodials and epipodials separately (limb bones were not pooled for independent contrasts). Second, ancestral character states (estimated using squared-change parsimony) were checked for the assumption of Brownian motion evolution that governs independent contrasts (Felsenstein, 1985; Díaz-Uriarte and Garland, 1996). This was performed by running assumption-testing operations in PDAP that evaluate the relationship between the absolute values of independent contrasts and their corresponding standard deviations. Non-significant relationships were determined for each of the data partitions, indicating that a Brownian motion model adequately fit the tip data. Finally, the same sets of regressions were performed on independent contrasts as in the untransformed data (size, robusticity, and vascular growth proxies).

PeerJ Reviewing Manuscript

Description

THEROCEPHALIA

Lycosuchidae

Lycosuchus vanderrieti

(Fig. 2)

General—SAM-PK-9084 (radius, ulna), from Reitkuil, Beaufort West (Middle Permian, *Tapinocephalus* AZ); SAM-PK-K9012 (femur), from Klein Koedoes Kop, Beaufort West (Middle Permian, *Tapinocephalus* AZ). The histological profiles of long bone shafts reveal well-vascularized cortical bone with multiple growth zones incorporating nonlamellar interstitial ECM (including woven- and parallel-fibered tissue) with reticular to subplexiform primary osteons, interrupted by cyclic growth marks (annuli or LAGs). Secondary osteons are apparently absent in all elements.

Radius—The radius (Fig. 2A, B) is a robust element with a circular cross-section at mid-diaphysis, revealing a compact cortex that grades into a porous spongiosa (the medullary region largely being occluded by cancellous bone). The bone wall thickness at the midshaft is moderate (*RBT*, 16%; *K*, 0.42) and composed of FLB with many large primary osteons. The osteons are arranged into both longitudinal and reticular orientations. The interstitial ECM is woven-fibered, but with some parallel-fibered tissue deposited periodically near growth marks. Intervening osteocyte lacunae are highly concentrated and disorganized between adjacent primary osteons and are generally globular in shape (resembling the ‘static osteogenic-derived woven bone’ of Stein and Prondvai, 2013). The densely packed longitudinal and reticular primary osteons are distributed in an ordered fashion within circularly organized growth zones. The canals become

PeerJ Reviewing Manuscript

smaller and more sparsely distributed in the outermost cortex where they are also predominantly longitudinal in orientation. The average mid-cortical vascularity (%*CV*) is 10.7 and the mean primary osteon diameter (*POD*) is 101 µm. Tissue structures, including growth marks, are well visible and there are at least three growth marks (LAGs) preserved in the cortex. The spacing of successive growth marks decreases toward the periosteal surface, and there is a strongly defined LAG in the outer region where the vasculature becomes more sparse and oriented longitudinally. Although apposition rate likely decreased toward the outer perimeter, there is no external fundamental system (EFS).

Ulna— The ulna (Fig. 2C) bears a broad, flat midshaft such that the cross-sectional profile is roughly ellipsoid to figure-8. As in the radius, the moderately porous cortex grades into a more cancellous medullary region that is largely occluded by fine cancellous bone and a few trabecular structures. The cortex is somewhat thicker than in the radius (*RBT*, 25%; *K*, 0.38). A small marrow cavity is present. The cortex consists of fibrolamellar structure, composed of primary osteons within a woven-fibered interstitial ECM but with some parallel-fibered tissue. The dense and disorganized lacunocanalicular network between primary osteons resembles that of the radius. The primary osteon orientation is predominantly reticular and radial. The %*CV* is 15.7 and the mean *POD* is 109 µm. The vascular canals (which are of moderate size) become finer and more sparsely distributed in the outermost cortex, indicative of growth attenuation. The vasculature is ordered within growth zones as in the radius, several of which can be discerned by well-defined LAGs. There are as many as four preserved LAGs in total. The LAGs become more closely spaced near the periosteal surface as in the radius. Although the outer region of the bone becomes more parallel-fibered, there is no EFS in the subperiosteal region.

PeerJ Reviewing Manuscript

PeerJ Reviewing Manuscript

Femur—The femur (Fig. 2D, E) is a short, robust bone with a compressed shaft that is oval in cross-section (unlike the rounded cross-section of later eutherocephalians). In section, the midshaft is of moderate thickness, but thinner than the forelimb elements (*RBT*, 15%; *K*, 0.67). It is composed of FLB with large primary osteons of varying orientations. The vascular motifs are somewhat complex, the predominant orientation being subplexiform, but with some reticular and radial osteons at muscular attachment sites, such as the adductor ridge. The degree of vascularization of the femur is generally greater than in the radius and ulna (%*CV*, 16.9; mean *POD*, 168 µm). Growth marks are difficult to distinguish due to the circular arrangement of primary osteons within the subplexiform network, although three faint bands (annuli?) of parallel-fibered bone can be observed in the posteroventral quadrant where the osteons form a more reticular arrangement. Faint bundles of Sharpey's fibers are also evident near the adductor ridge in the outer cortex, indicating attachment of the adductor musculature. The matrix composing the outermost cortex is highly birefringent, indicative of its strong parallel-fibered and lamellar structure. The lacunocanalicular network also includes more lenticular osteocyte lacunae that are sparsely distributed. Although the bone being laid down in this region was no longer fibrolamellar and the vascular canals became sparser, the tissue lacks the avascular and multi-lamellar structure characteristic of a true EFS.

SCYLACOSAURIA

Scylacosauridae

Glanosuchus macrops

(Fig. 3A)

General—BP/1/6228 (ulna), from the Grant, Albany (Middle Permian, *Tapinocephalus* AZ).

Ulna—The ulna (BP/1/6228) is a relatively flat element with an ellipsoid to figure-8 cross-section along the midshaft. The bone is relatively dense with a highly cancellous internal structure deep to the cortex with poor development of the marrow cavity. The cortex is moderately thick (*RBT*, 20%; *K*, 0.42) and composed of fibrolamellar and parallel-fibered bone with primary osteons, periodically interrupted by growth marks. Localized areas contain lenticular osteocyte lacunae, particularly in the outer cortex, although the majority of osteocyte lacunae are globular and haphazardly organized. Secondary structure is limited; secondary osteons are apparently absent, but resorption cavities formed in the deep cortex near the compact-cancellous transition. The vascular network is predominantly made up of longitudinal primary osteons, which are distributed most densely in the anterior (preaxial) and posterior (postaxial) sides of the bone where the growth zones are thickest. The longitudinal primary osteons are generally largest deeper in the cortex, and become smaller and more sparsely distributed in the outer cortex, closest to the subperiosteal region. However, in the outer cortex along the anterior and posterior margins, the primary osteons generally maintain their size and form a slightly more reticular motif. The %*CV* is 4.9 and the average primary osteon diameter is 51 μm, therefore having a comparatively lesser degree of vascularization than in *Lycosuchus*. Growth zones delimited by opaque growth marks are easily distinguishable in the specimen. There are at least three annuli traceable around the bone. Their spacing does not decrease toward the periphery, and the outermost growth zones maintain moderate vascularity with reticular FLB in some areas. Primary osteons were still forming in the subperiosteal region and no EFS was laid down by the time of death.

PeerJ Reviewing Manuscript

Scylacosauridae indet.

(Fig. 3B-E)

PeerJ Reviewing Manuscript

General—BP/1/5576 (radius, ulna), from Combrinckskraal, Prince Albert District (Middle Permian, *Tapinocephalus* AZ); BP/1/5587 (humerus, radius, ulna), from Wolwekuil, Victoria West (Middle Permian, *Tapinocephalus* AZ); CGS R300 (humerus), locality unknown; SAM-PK-5018 (humerus, radius, femur, tibia, fibula), from Abrahamskraal, Prince Albert District (Middle Permian, *Tapinocephalus* AZ); SAM-PK-11557 (fibula), from De Cypher, Beaufort West (Middle Permian, *Tapinocephalus* AZ). Long bone microstructure has been described in scylacosaurids (Ricqlès, 1969; Ray, Botha & Chinsamy, 2004; Chinsamy-Turan, 2012), but previous genus-level identifications of these specimens are dubious due to inadequate diagnostic skull material. As two of the studied specimens have been described elsewhere (SAM-PK-5018, 11557) the present analysis serves to supplement these earlier descriptions with additional material.

Humerus—The humerus is a robust bone with a thick cortex at midshaft (*RBT*, ~30%; *K*, ~0.30) and an open marrow cavity with a few coarse trabeculae and lined by endosteal lamellae. The cortex is composed predominantly of FLB with densely packed primary osteons having a variety of orientations in localized regions. Ray, Botha & Chinsamy (2004) reported a laminar to subplexiform arrangement of osteons with occasional subreticular osteons in localized regions, corroborated here by study of additional specimens (BP/1/5587, CGS R300). Independent observations suggest that a subplexiform pattern of vascularization in the humerus midshaft was characteristic of scylacosaurids, but with strongly oblique or reticular patterns localized near

PeerJ Reviewing Manuscript

sites of muscle insertion that are also associated with Sharpey's fibers (i.e., deltopectoral crest). No secondary osteons are present in the humerus. The %*CV* is ~13-15% and the average primary osteon diameter bears a wide range of ~75-112 μm, which is generally high for therapsids. The interstitial ECM is more parallel-fibered than woven and the primary osteons are lined by thick circumferential lamellae, so that there is strong birefringence under crossed-polarized light. Osteocyte lacunae are well concentrated, globular and disorganized, but are more lenticular where they are associated with streaks of parallel-fibered bone preceding growth marks. Parallel-fibered bone is common in growth increments immediately preceding growth marks (LAGs), indicating decelerating growth before periodic cessation. The number of preserved growth marks varies among individuals, but ranges from three to five LAGs.

Radius—The radius midshaft is subtriangular in cross-section and bears a moderately thick bone wall (*RBT*, ~17-23%; *K*, ~0.46-0.47) with an open marrow cavity lined by sparse trabecular structures, but generally with a sharp delineation of the cortex. Primary osteons are scattered throughout the cortex in a predominantly longitudinal orientation, though canals are more obliquely radial in localized areas such as the attachment site of the interosseous membrane. The interstitial ECM is more parallel-fibered than woven and punctuated by occasional growth marks. Areas of parallel-fibered bone bear more sparsely distributed and ordered lenticular osteocyte lacunae, especially in the outer cortex and near growth marks. In BP/1/5587, the exact number of growth marks is difficult to discern and the outer layers of bone appear to have been actively deposited during the time of death (with primary osteons forming around the subperiosteal region). By contrast, BP/1/5576 exhibits four or more growth marks that appear in the outer half of the cortex and become progressively closer spaced toward the

subperiosteal margin, indicating that growth had slowed prior to death in spite of its smaller size compared to BP/1/5587. However, there was no EFS as in the other studied elements.

Ulna—The histological profile of the ulna is near identical to the radius, although the oblate nature of the bone with wider growth zones allows the number of growth marks to be more reliably estimated. BP/1/5587 exhibits at least three thick growth zones with sparse longitudinal and reticular osteons and weakly radial osteons along the expanded anterior and posterior sides of the bone. These osteons were still being formed at the time of death, corroborating the observations from the radius of the same individual. BP/1/5576 differs in that as few as five (and as many as six) growth marks accompanied by incremental lamellae (annuli) are apparent in the outer cortex, becoming closer spaced toward the subperiosteal margin as in the radius. The primary osteons are longitudinally oriented with occasional subreticular orientations in some areas. Among-individual histovariation suggests the existence of variation in subadult growth rates within these two scylacosaurids.

Femur—The femur of SAM-PK-5018 was described by Ray, Botha & Chinsamy (2004). It bears a relatively thin bone wall compared to the forelimbs that is composed of moderately vascularized FLB. The primary osteons are predominantly longitudinal to subreticular in orientation. The perimedullary region bears extensive resorption cavities and a few secondary osteons as reported by Ray, Botha & Chinsamy (2004). There were apparently no growth marks preserved in the specimen.

Tibia—The tibia (SAM-PK-5018) is a thick bone, though with an open marrow cavity and moderately thick bone wall as in the forelimb epipodial elements (*RBT*, 24%; *K*, 0.60), but thinner than the humerus. The cortex is predominantly composed of FLB with subreticular primary osteons as described by Ray, Botha & Chinsamy (2004). Additionally, there are at least

PeerJ Reviewing Manuscript

three growth marks visible (a faint inner annulus and two sharply defined LAGs in the outer cortex) demarcating growth zones of variable thicknesses. Toward the periphery the primary osteons become more obliquely oriented, taking on a strong radial orientation in the outer two growth zones and communicating with the periosteal surface (indicating active bone growth at the time of death). The lacunocanalicular network is too poorly preserved to be described and osteocyte lacunae are not discernible. Secondary osteons are absent.

Fibula—The fibula is extremely poorly preserved in SAM-PK-5018, primarily due to obliteration of the outer cortical surface, thereby making growth interpretations difficult. Deep portions of the cortex in this specimen reveal large erosion cavities and secondary osteons. Discussion of primary growth in the fibula is herein limited to SAM-PK-11557, which preserves a thick cortical wall with coarse trabeculae surrounding a marrow cavity. Resorption cavities are extensive throughout the perimedullary region and are lined endosteally by lamellar bone. The fibrolamellar cortex is densely compacted with large, infilled primary osteons tightly packed and predominantly longitudinal in orientation (though with sparse reticular osteons and anastomoses). The lacunocanalicular network between osteons is formed by haphazardly arranged globular osteocyte lacunae. The exact number of growth marks is difficult to discern, but a relatively thick growth zone with abundant primary osteons gives way to a series of closely spaced annuli near the periphery. The vasculature in this outer region also became sparse, suggesting an overall decrease in growth prior to death. Osteocyte lacunae in this region were more sparse and lenticular in shape. Secondary osteons are occasionally present in the deep cortex, diagnosed clearly by their scalloped cement lines (Fig. 3B).

PeerJ Reviewing Manuscript

EUTHEROCEPHALIA

Akidnognathidae

Olivierosuchus parringtoni

(Fig. 4A-C, E, F)

PeerJ Reviewing Manuscript

General—NMQR 3605 (humerus), from Barendskraal, Middleburg (Lower Triassic, *Lystrosaurus* AZ); SAM-PK-K10617 (femur), from Wapadsberg Pass, Zeekoegat, Graaff-Reinet District (Lower Triassic, *Lystrosaurus* AZ). The cross-sectional profiles of limb bone shafts in *Olivierosuchus* reflect general tendencies in other therocephalians, in that the forelimb was robust and thick-walled whereas the hindlimb was relatively gracile and thinner-walled (the humeral cortex being extremely thickened and marrow cavity occluded; the femur having a relatively open marrow cavity with few trabeculae). The cortex predominantly incorporates a nonlamellar interstitial ECM with dense, reticular vascularization as in *Moschorhinus* (Huttenlocker and Botha-Brink, 2013). Growth marks are few and confined to the outer cortex and secondary reconstruction is limited. There are no secondary osteons.

Humerus—The humerus (NMQR 3605) (Fig. 4A-C) bears a prominent deltopectoral crest that traverses most of the length of the shaft, producing a subtriangular or tear-shaped cross-section as in *Moschorhinus* and other medium-to-large therocephalians. Notably, the bone is extremely compacted in section and most of the medullary region is occluded by coarse trabeculae such that the marrow cavity is extremely reduced (approximate radius of cavity ~ 2 mm). As a result, the cortex is extremely thick (*RBT*, 36%; *K*, 0.38). The cortical bone consists of both longitudinal and reticular primary osteons in a woven-fibered interstitial ECM, although the matrix becomes more parallel-fibered in the outer half of the cortex. The large, intervening

PeerJ Reviewing Manuscript

osteocyte lacunae between osteons are numerous between primary osteons, highly concentrated and almost exclusively globular in shape. The cortical bone is moderately well-vascularized and the primary osteons are large (%*CV*, 9.9; mean *POD*, 99 μm). Several of these features resemble *Moschorhinus*, including the occluded lumen, disorganized woven-fibered matrix, abundant reticular canals, and large primary osteons. Kitching (1977) suggested that *Olivierosuchus* might represent a juvenile of *Moschorhinus*. However, the specimen NMQR 3605 is interpreted here as near somatic maturity as suggested by Botha-Brink and Modesto (2011). It is the largest known specimen of its kind (BSL = 122 mm), exhibits fused neurocentral sutures, and records the transition to outer parallel-fibered bone in the humeral cortex with two distinct LAGs. This contrasts with the condition in a slightly larger *Moschorhinus* specimen from coeval Triassic rocks (SAM-PK-K118) which shows heavily vascularized FLB with no growth marks (Fig. 4C, D).

Femur—The femur (SAM-PK-K10617) (Fig. 4E, F) is more elliptical in cross-section, although some dorsoventral compression has distorted the shaft slightly, flattening and cracking it. The cortical bone is relatively well preserved, revealing a somewhat thinner diaphyseal bone wall than in the humerus. Some coarse cancellous bone is present around the perimedullary region. The cortex is composed of FLB with longitudinal primary osteons. Osteocyte lacunae are large, highly concentrated and haphazardly distributed. There is a moderate to weak degree of vascularization, although the osteons are relatively large (%*CV*, 3.4; mean *POD*, 75 μm). The interstitial ECM is predominantly woven-fibered but with some patches of parallel-fibered bone in the outer cortex. There are no growth marks visible in the specimen and no secondary osteons.

Hofmeyriidae

Hofmeyria atavus

(Fig. 5)

PeerJ Reviewing Manuscript

General—BP/1/4404 (humerus, radius, ulna), from Matjiesfontein (Highlands), Victoria West (Upper Permian, *Cistecephalus* AZ). The bones are remarkably robust and thick-walled relative to the size of the individual (BSL = 67 mm). The cross-sectional profile of the mid-diaphysis in all bones includes a distinct central cavity with a smooth, circular rim of endosteal lamellar bone (rather than irregularly organized cancellous bone tissue). The tissue composition of the cortex is generally more parallel-fibered than woven and the outer cortex of the epipodials preserves numerous annular growth marks. Primary osteons are primarily longitudinally oriented (though with many reticular connections in the humerus) and mostly reside in the inner half to two-thirds of the cortex. There are no secondary osteons in any of the studied elements.

Humerus—The humeral diaphysis (Fig. 5A) bears a relatively compact cross-sectional profile as in most of the other elements, given its thick cortex (*RBT*, 31%; *K*, 0.32) and sharp boundary between the cortical bone wall and the diminutive central cavity. There are a few coarse trabeculae around the marrow cavity, rather than the extensive cancellous tissue observed in earlier therocephalians. The interstitial ECM of the cortical bone appears to incorporate some woven-fibered structure, but is primarily parallel-fibered, especially nearing the subperiosteal margin. Osteocyte lacunae are primarily large, globular, and well-concentrated. The primary osteons are fairly densely-packed throughout much of the cortex and form a reticular network with occasional longitudinal canals. The cortex is moderately vascularized, although the primary osteons are relatively small (%*CV*, 7.5; mean *POD*, 72 μm). Growth marks are not easily

distinguishable in the humerus. However, when viewed under polarized light, three bundles or 'waves' of highly birefringent parallel-fibered bone are visible in the outer half of the cortex, possibly indicating cyclic alternations in rate of bone accretion. Parallel-fibered bone predominates in the outer cortex, but still incorporates abundant primary osteons.

Radius—The radius (Fig. 5B-D) generally resembles the humerus in its overall cross-sectional profile, but with a thicker bone wall and more diminutive marrow cavity (*RBT*, 35-40%; *K*, 0.15-0.26) as is typical of the epipodial elements. The small central cavity is lined by a thick, multi-lamellar layer of endosteal bone. The total diameter of the cavity varies between 0.25-0.50 mm. The cortical bone is composed of a predominantly parallel-fibered bone matrix with sparse primary osteons. The lacunocanalicular network was also somewhat sparse and osteocytes became increasingly lenticular in shape toward the outer margin of the bone. The primary osteons are mainly oriented longitudinally, but with a few reticular connections. They are concentrated in the inner half to two-thirds of the cortex and become very sparse in the outer cortex, where the vasculature mainly consists of a few simple canals. The overall degree of vascularization is quite low (%*CV*, 3.4-4.8; mean *POD*, 46-47 μm). Growth marks are better recorded in the epipodials than in the humerus of BP/1/4404. At least three (and possibly four) growth marks are preserved throughout the cortex, although their precise number is difficult to count due to their association with fine incremental lines. Association of incremental lamellar bone and a lack of sharply defined cement lines indicate that these waves of growth marks represent annuli (as opposed to LAGs) marking periodic decelerations in growth rather than cessations. The growth marks become more closely spaced in the subperiosteal region, but do not form an avascular EFS (as suggested by the presence of simple canals).

PeerJ Reviewing Manuscript

Ulna—Apart from its more flattened cross-sectional shape, the ulna (Fig. 5E, F) is near identical to the radius in its histological profile and tissue structures. The cortical bone wall is similarly thick (*RBT*, 39%; *K*, 0.20-0.22) and dominated by parallel-fibered bone with longitudinal primary osteons and cyclic growth marks (annuli). Osteocyte lacunae are sparse and strongly lenticular in shape in the outer cortex as in the radius. The cortex is also only modestly vascularized (%*CV*, 3.0-4.7; mean *POD*, 39-43 μm). Some osteons in regions where the bone wall is relatively thinner have the gross appearance of secondary osteons (Fig. 5E). However, this is mainly due to their large size and multi-lamellar infilling. Close inspection reveals that there is no cement line surrounding these osteons, and that the surrounding fabric of the interosteonal ECM also conforms to their shape. Secondary osteons are therefore absent.

Mirotenthes digitipes

(Fig. 6)

General—SAM-PK-K6511 (humerus, radius, ulna, femur, tibia, fibula) from Steenkampshoek (Upper Permian, *Cistecephalus* AZ). As in *Hofmeyria* (BP/1/4404), limb bone shafts are thick-walled for their small size, and the cortex is composed of moderately vascularized FLB with primary osteons (and simple canals) and a predominantly parallel-fibered interstitial ECM. Cyclic growth marks are present throughout the cortex, especially toward the outer periphery. The subperiosteal region of some elements preserves more parallel-fibered or lamaller bone with sparse vascular canals. Secondary osteons are absent in all elements.

Humerus—The humerus shaft (Fig. 6A) exhibits a compact cross-sectional profile with a thick bone wall (*RBT*, 32; *K*, 0.31) and a small central cavity with a slightly irregular endosteal

PeerJ Reviewing Manuscript

PeerJ Reviewing Manuscript

margin and some trabecular structures occupying the cavity. The cortex incorporates numerous primary osteons within a predominantly parallel-fibered interstitial ECM. Osteocyte lacunae were well-concentrated and became increasingly lenticular toward the periphery of the bone. The vasculature is very simple in its organization, mainly consisting of many sparsely distributed longitudinal primary osteons and occasional simple canals (%*CV*, 5.4; mean *POD*, 54 μm). The primary osteons occasionally (though infrequently) bear radial and circular anastomoses, especially deeper in the cortex. Closer to the periphery, primary osteons become fewer and give way to simple canals of varying orientations. Growth marks are more clearly delineated in this humerus than in that of BP/1/4404, and are best visualized in normal (non-polarized) light. Three evenly spaced growth marks are present in the mid-cortex, and a fourth in the subperiosteal region. As in BP/1/4404, growth marks are preserved in the form of annuli, and are associated with faint incremental lines and waves of birefringent parallel-fibered bone when viewed under polarized light. There is no EFS.

Radius—The radius (Fig. 6B) has a similarly thickened bone wall at midshaft (*RBT*, 34; *K*, 0.33) with a small but relatively open central cavity. The cavity is unobstructed by trabecular or cancellous structures, instead lined by a smooth layer of endosteal lamellar bone, and is approximately 0.80 mm in diameter. The cortex is formed primarily by parallel-fibered bone that is modestly vascularized by sparse primary osteons and simple canals (%*CV*, 3.5; mean *POD*, 38 μm). The lacunocanalicular network is poorly preserved in this element, but osteocyte lacunae apparently became more sparse in the outer cortex. Most of the vascular network is localized within the inner half of the cortex (but with a few simple canals present in the outer half). At least five annuli are present, more distinct than in the humerus, and are very closely spaced in the outer cortex forming an EFS-like structure that is nearly avascular, but not acellular.

PeerJ Reviewing Manuscript

Ulna—The histological profile of the ulna (Fig. 6C) is near identical to that of the radius, except for its more flattened, ellipsoidal shape in section. The bone wall is thick (*RBT*, 32; *K*, 0.42), the cortex is composed of parallel-fibered bone with many small primary osteons (%*CV*, 2.0; mean *POD*, 41 μm), and at least four or five growth marks (annuli) are present throughout the cortex. Osteocyte lacunae became increasingly sparsely distributed in the outer cortex.

Femur—The femur midshaft (Fig. 6D) resembles the humerus in its overall cross-sectional profile and distribution of histological features, although it is slightly thinner-walled than any of the forelimb elements (*RBT*, 25; *K*, 0.42). There is a wide, open marrow cavity with some trabeculae and erosion cavities forming within the surrounding deep cortex. A thin layer of lamellar bone lines the endosteal margin of the cortex. The deep cortex is formed by moderately vascularized FLB, consisting of a parallel- and woven-fibered matrix with longitudinally oriented primary osteons. The lacunocanalicular network is sparse and osteocytes became more lenticular in shape in the outmost cortex. The primary osteons are more consistently longitudinal than in the humerus, with fewer anastomoses, but the overall degree of vascularization is comparable (%*CV*, 3.6; mean *POD*, 58 μm). Primary osteons become fewer in the outer cortex, but are still present with few simple canals. Growth marks are present throughout the cortex, but are best seen in the outer regions where primary osteons are less densely concentrated and parallel-fibered bone dominates. There are at least four growth marks, which become progressively closer spaced toward the periphery as in the humerus. There is no EFS in this element.

Tibia—The tibia (Fig. 6E) exhibits an irregular, slightly figure-8 cross-sectional shape and a relatively thick bone wall (*RBT*, 31; *K*, 0.31) as in the other epipodial elements. The marrow cavity, however, is also irregular in shape with coarse trabeculae and occasional small

resorption cavities forming along the endosteal margins. The cortex is formed by parallel-fibered bone with small, longitudinally and radially oriented primary osteons that are most concentrated in the deep cortex. The lacunocanalicular network is too poorly preserved for adequate description. The overall degree of vascularization is fairly modest (%*CV*, 3.1; mean *POD*, 38 μm). Numerous growth marks are preserved in the outer cortex, especially near the subperiosteal region where they form a nearly avascular EFS-like structure as in the radius.

Fibula—The fibula (Fig. 6F), apart from being more triangular in cross-section, resembles the tibia in its overall histological profile. It has a thick bone wall at midshaft (*RBT*, 32; *K*, 0.39) with some trabecular architecture in the marrow cavity. The cortex is formed by parallel-fibered bone with few longitudinally oriented primary osteons, and is poorly vascularized (%*CV*, 3.9; mean *POD*, 32 μm). Osteocyte lacunae are poorly preserved as in the tibia. Growth marks are faint, but an avascular EFS-like structure forms a distinctive collar around the bone.

Whaitsiidae

Theriognathus microps

(Fig. 7)

General—BP/1/719 (femur) from Swaelkrans, Murraysburg District (Upper Permian, *Dicynodon* AZ); NMQR 3375 (femur) from Tafelkop 712, Bloemfontein District (Upper Permian, *Dicynodon* AZ). The histological structure of the radius in *Theriognathus* has previously been described by Ricqlès (1969) (as '*Notosollasia'*). The specimen was recovered from the Doornplaats locality (*Dicynodon* AZ) where this taxon occurs abundantly. Based on the

PeerJ Reviewing Manuscript

author's detailed descriptions and photographic plates, the structure of the radius midshaft resembles that of the hofmeyriids described above in having an extremely thick bone wall and reduced central cavity (Ricqlès, 1969). The vascular motif was primarily longitudinal and radial. Secondary osteons are absent in all studied specimens.

Femur—Two femora are described here to supplement the description by Ricqlès (1969). It is worth noting that the femur of *Theriognathus* is unique in its strongly golf club-shaped head that fits into a deep acetabulum, and a bowed shaft that orients the distal condyles directly ventrally, placing the lower leg under the hip in a semi-erect stance. The midshaft is rounded in cross-section and bears a relatively thick wall (*RBT*, ~20-24%; *K*, ~0.51-0.59) compared to the hind limbs of other therocephalians, possibly related to impact loading imposed by this orientation. The thick cortical bone wall is composed of cyclically deposited FLB with numerous primary osteons in a parallel- and woven-fibered matrix. Osteocyte lacunae are generally numerous, haphazardly distributed, and globular in shape within growth zones, but more lenticular and ordered near growth marks. In the small subadult specimen sampled here (NMQR 3375), primary osteons are abundant and take on a predominantly radial orientation, but with a few longitudinal osteons arranged in radial rows or bearing radial and reticular ramifications. Numerous growth marks (LAGs) record a cyclic growth pattern, with five irregularly spaced growth marks punctuating the cortex in NMQR 3375, followed by a thick, well vascularized growth zone in the outermost cortex indicating a brief 'spurt' prior to death. In the larger femur (BP/1/719) there is a lesser degree of radial vasculature, the primary osteons being almost exclusively longitudinal (although with some reticular anastomoses in the outer cortex). In general, the cortex bears a moderate degree of vascularization (%*CV*, 6.2-6.8; mean *POD*, 65-87 μm). BP/1/719 preserves at least four growth marks, although its early growth

PeerJ Reviewing Manuscript

record has been lost by formation of resorption cavities in the perimedullary region. The number and spacing of growth marks suggests some degree of plasticity in the growth style of *Theriognathus*.

PeerJ Reviewing Manuscript

BAURIOIDEA

Ictidosuchidae

Ictidosuchoides longiceps

(Fig. 8)

General—BP/1/75 (humerus), from Sondasgriviershoek, Cambedoo, Graaff-Reinet District (Upper Permian, *Cistecephalus* AZ); BP/1/4092 (humerus, radius, ulna) from Matjiesfontein, Victoria West (Upper Permian, *Cistecephalus* AZ); SAM-PK-K8659 (humerus, radius, femur, tibia, fibula) from Wilgerboskloof, Prince Albert District (Upper Permian, *Tropidostoma* AZ); SAM-PK-K10423 (femur, tibia, fibula) from Doornplaats, Graaff-Reinet District (Upper Permian, *Dicynodon* AZ). The specimens present a variety of sizes and ages, ranging from the small skeleton SAM-PK-K8659 (BSL = 101 mm), which bears neurocentral sutures, to the largest known specimen BP/1/4092 (BSL = 200 mm). Mid-diaphyseal sections reveal somewhat thinner bone walls in *Ictidosuchoides* (and perhaps baurioids in general) than in other therocephalians with *RBT*s generally ranging from 14-26% (rather than 25-40% in akidnognathids and hofmeyriids). The cortices are formed by moderately vascularized parallel-fibered bone with reticular and longitudinal primary osteons, and punctuated by cyclic growth marks. There are no secondary osteons.

PeerJ Reviewing Manuscript

Humerus—The humerus (Fig. 8A, G, H) is a slender bone with a well-defined shaft having a subcircular cross-sectional profile. The overall compactness of the bone is low with a fairly thin bone wall (*RBT*, ~19-22%; *K*, ~0.56-0.64). The marrow cavity is large and relatively hollow with little cancellous structure (a few trabeculae are present in proximal shaft of BP/1/75). The endosteal perimedullary margin is smooth at the midshaft. Resorption cavities are near absent in the perimedullary region. The remaining cortex generally consists of reticular FLB in a parallel- and woven-fibered matrix. Osteocyte lacunae are generally numerous and disorganized with a globular shape in growth zones, but more lenticular and ordered near growth marks as in the femur of *Theriognathus*. The reticular primary osteons occasionally bear circular anastomoses that give a subplexiform appearance in localized regions of the cortex. The osteons are quite small, but the bone is moderately well vascularized overall (%*CV*, ~7.3-11.1; mean *POD*, ~45-60 μm) with most of the osteons being concentrated within the deep cortex. Cyclic growth marks are faint but present, usually in the form of annuli with associated waves of 'streaky' parallel-fibered bone as in the hofmeyriids. The number of growth marks varies, with a single subperiosteal annulus in the small SAM-PK-K8659, two faint annuli preserved in the medium BP/1/75, and three annuli in the largest BP/1/4092. Growth apparently did not fully cease in the largest individual, but more parallel-fibered and lamellar bone formation occurred in the outer half of the cortex, with more lamellar fibers and flattened osteocyte lacunae appearing after the third (outermost) annulus.

Radius—The radius (Fig. 8B, I), like the humerus, bears a slender shaft having a bone wall of moderate thickness (*RBT*, ~21-24%; *K*, ~0.52-0.58), contrasting with the forelimb epipodials of other non-baurioid therocephalians. The endosteal perimedullary margin is relatively smooth at the midshaft and there are few trabeculae within the marrow cavity. The

PeerJ Reviewing Manuscript

cortical bone wall is composed of FLB with small, longitudinal primary osteons and the interstitial ECM apparently became increasingly parallel-fibered toward the outer periphery. Osteocyte lacunae are generally numerous and disorganized, and globular in shape, but became sparser and more lenticular near growth marks and in the outer cortex of large individuals. Osteons are very small and mostly longitudinal, but exhibit occasional reticular motifs. The transition to parallel-fibered bone occurred early during the bone's growth, as it is evident in the smallest specimen (SAM-PK-K8659) where bundles of parallel-fibered bone were deposited just prior to formation of a subperiosteal annulus (as in the humerus). The larger BP/1/4092, retains a similar pattern, with alternating waves of deposition of parallel-fibered bone concentrated near three faint annuli moving toward the outer periphery. The size and concentration of primary osteons also decreases toward the periphery and overall vascularity is moderate to low (%*CV*, ~4.2-11.1; mean *POD*, ~38-62 μm). No more than three growth marks are observed throughout the cortex in the largest specimens and there is no EFS.

Ulna—The ulna (BP/1/4092) forms a flattened diaphysis with an oval cross-section and a bone wall that is of moderate thickness (*RBT*, 26%; *K*, 0.54). The marrow cavity is large with an irregular endosteal margin and several trabeculae present within the cavity. The structure of the cortex closely resembles the radius, being composed of FLB with small, longitudinal and reticular primary osteons and occasional streaks of parallel-fibered bone when viewed under polarized light. As in the radius, osteocyte lacunae are disorganized and globular, but became sparser and more lenticular near growth marks and in the outer cortex. Frequent reticular canals are present throughout the preaxial region of the cortex, forming primary osteons of moderate size in a woven- and parallel-fibered matrix incorporating dense clusters of globular osteocyte lacunae. The overall %*CV* is 8.3 and the mean *POD* is 52 μm. Growth marks, though present, are

difficult to distinguish due to poor preservation, and a complete count cannot be performed. At least one distinct annulus can be observed in the outer two-thirds of the cortex, but there were likely more given those recorded in the radius and humerus of the same individual.

Femur—The femur (Fig. 8D, E) bears a long, straight shaft that is thinner walled than in any of the forelimb elements (*RBT*, 14%; *K*, 0.71). The marrow cavity is very large with an irregular boundary of coarse, trabecular bone between it and the more compact cortex. In the small SAM-PK-K8659, prominent trabecular structures are present along the perimedullary margins and large cavities (~60-100 μm in diameter) not interpreted as erosion cavities are surrounded by highly woven bone before giving way to a very thin layer of woven- and parallel-fibered bone with primary osteons in the outmost region of the mid- and distal shaft. The highly woven texture preserved in the perimedullary region resembles the endochondral scaffold of perinatal bone in mammals and some archosaurs (Horner et al., 2001). In general, the primary osteons are fairly small and have both longitudinal and radial orientations (%*CV*, 4.7; mean *POD*, ~38-65 μm). Parallel-fibered bone became more prominent in the outermost regions of the midshaft in SAM-PK-K10423. The lacunocanalicular network is poorly preserved in both femur specimens. A possible subperiosteal annulus was formed in SAM-PK-K10423, but no growth marks were otherwise detected in either specimen. Some obliquely oriented Sharpey's fibers are preserved on the ventral surface of the distal shaft. No EFS was observed in the femur.

Tibia—The tibia (Fig. 8C) exhibits a structure similar to the radius and ulna. It bears a flattened cross-section with a modest bone wall (*RBT*, ~16-23%; *K*, ~0.49-0.63). The small SAM-PK-K8659 records the same transition between the porous, woven perimedullary bone and parallel-fibered cortical bone as in the radius and femur. The cortex is composed of parallel-fibered bone with small longitudinal and reticular primary osteons and some intervening

PeerJ Reviewing Manuscript

Sharpey's fibers preserved in the anterior region in SAM-PK-K8659. The cortex is poorly vascularized (%*CV*, 2.8-4.3; mean *POD*, 39-43 μm). Two annuli are preserved in the cortex of SAM-PK-K10423. There is no EFS.

Fibula—The fibula (Fig. 8F) exhibits a subcircular cross-section, and resembles the tibia in its histological profile. The bone wall is moderately thin at the midshaft (*RBT*, ~19-22%; *K*, ~0.47-0.59) and retains some of the porous, woven architecture in the perimedullary region as observed in the radius, femur, and tibia of SAM-PK-K8659. The transition to the compact cortex is marked by a sharp cement line, followed by deposition of sparsely vascularized parallel-fibered bone as in the tibia. The overall vascularization is fairly modest (%*CV*, ~3.8-4.7; mean *POD*, 40 μm). The primary osteons are longitudinally oriented and there are a few simple canals. Growth marks are not distinguishable in the fibula and there is no EFS.

Lycideopidae

Tetracynodon darti

(Fig. 9)

General—NMQR 3745 (humerus), from Bethal, Bethulie District (Lower Triassic, *Lystrosaurus* AZ); UCMP 78395 (humerus, radius, ulna, femur), from Wonderkrantz, Harrismith District (Lower Triassic, *Lystrosaurus* AZ); UCMP 78396 (humerus, femur, fibula), from Wonderkrantz, Harrismith District (Lower Triassic, *Lystrosaurus* AZ). Sigurdsen et al. (2012) briefly described bone histology in the humerus and femur of *Tetracynodon* with the purpose of determining relative age. The bone walls are generally thin (as in other baurioids), especially in the femur. In all elements, the mid-diaphyseal cortex consists of moderately vascularized woven-

PeerJ Reviewing Manuscript

and parallel-fibered bone, usually with longitudinal primary osteons. The cortices are, in general, less vascularized than in its Permian counterpart *Ictidosuchoides*. Growth marks are often absent indicating a relatively short growth period in sampled specimens, although there may be one or two preserved in the mid- to outer cortex in some specimens. Secondary reconstruction was limited and there are no secondary osteons.

Humerus—The humerus (Fig. 9A-C) exhibits an intermediate bone wall thickness (*RBT*, ~21-24%; *K*, ~0.49-0.56) and preserves well the general pattern of growth. The large, open marrow cavity is bordered by smooth endosteal lamellar bone, demarcating the transition to the cortex. There are occasional trabecular structures localized in the proximal shaft near the deltopectoral crest. The crest is more restricted along the shaft than in earlier (non-baurioid) therocephalians, such that the cross-section is more subcircular than tear-shaped. The cortex consists of moderately vascularized woven- and parallel-fibered bone incorporating longitudinal primary osteons with occasional reticular anastomoses (%*CV*, ~4.7-8.1; mean *POD*, ~36-42 μm). The deep cortex maintains a clear fibrolamellar structure with densely-packed primary osteons within a woven-fibered interstitial ECM. The lacunocanalicular network of the deep cortex is generally disorganized with large, globular osteocyte lacunae, but quickly transitioned to more ordered, lenticular osteocytes in the outer half of the cortex. The cortical bone of *Tetracynodon* bears the highest proportion of ordered, lenticular osteocytes than any studied therocephalian. In NMQR 3745, this pattern gave way to more parallel-fibered bone with lenticular osteocytes in the outer half of the cortex. This transition is demarcated by a single LAG, although a second faint annulus associated with bundles of parallel-fibered bone is present in the outer cortex. Other specimens (e.g., UCMP 78395, 78396) show more consistent parallel-fibered bone deposition. The outer cortex incorporates lamellar tissue with fewer vascular canals and is

PeerJ Reviewing Manuscript

punctuated by a single LAG near the subperiosteal region. The LAG is succeeded by a thin band of parallel-fibered and lamellar bone (varying from ~50 to 100 μm) with few simple canals located near the periosteal margin, indicating that although growth had attenuated it had not fully ceased. No EFS is present in any of the specimens.

Radius—The radius (UCMP 78395) (Fig. 9D) has a subcircular cross-section at midshaft and bears a slightly thicker bone wall than in the humerus (*RBT*, 27%; *K*, 0.43). The perimedullary region bears a relatively smooth ring of endosteal lamellar bone marking the border with the marrow cavity. A few resorption cavities are present in the perimedullary region, especially near the postaxial region of the bone. This region also preserves abundant Sharpey's fibers throughout much of the cortex. The cortex is predominately formed by poorly vascularized parallel-fibered bone with primary osteons and simple canals (%*CV*, 1.9; mean *POD*, 42 μm). Osteocyte lacunae are globular in shape and haphazardly arranged, but are sparsely distributed and became more lenticular in some areas of the outer cortex. The sparse vascular canals bear an exclusively longitudinal orientation. Growth marks appear to be absent in the studied specimen.

Ulna—The ulna (UCMP 78395) is similar to the radius in its histological profile, although it is more flattened and bears more trabecular architecture in the marrow cavity. The bone wall is somewhat thicker (*RBT*, 31%; *K*, 0.33) and the transition between the marrow cavity and the cortex is irregular and less abrupt. Large resorption cavities are present in the perimedullary region and the inner half of the cortex exhibits abundant woven-fibered tissue. The lacunocanalicular network is sparse as in the radius, with osteocytes becoming fewer and more lenticular in the outer cortex. The vasculature becomes extremely sparse in the outer cortex (%*CV*, 2.8; mean *POD*, 38 μm) where there is also more parallel-fibered bone. Vascular canals

PeerJ Reviewing Manuscript

are almost exclusively longitudinal as in the radius, although there are a few reticular canals. Growth marks are apparently absent in the ulna and there is no EFS.

Femur—The femur (Fig. 9E, F) has a slender shaft that is subcircular in section, exposing a thin bone wall and a large, open marrow cavity (*RBT*, 17%; *K*, 0.66). The transition between the marrow cavity and the cortex is abrupt, demarcated by a smooth layer of endosteally deposited lamellar bone. The composition of the cortex is similar to that of the humerus, although there is more woven-fibered tissue. As in the humerus, the osteocyte lacunae are frequently lenticular in shape, but are somewhat less ordered. The cortex is dominated by FLB having woven- and parallel-fibered interstitial ECM and numerous small primary osteons (%*CV*, ~4.3-5.0; mean *POD*, ~39-42 μm). The primary osteons are both longitudinal and reticular. In UCMP 78396, there is a transition to parallel-fibered and lamellar bone in the outermost cortex that is associated with a possible annulus. This transition is also associated with a decrease in the size and concentration of vascular canals toward the subperiosteal surface. Growth marks are otherwise absent from the cortex and there is no true EFS. In addition to cross-sectional sampling, longitudinal sections were possible across the head of the femur in UCMP 78396, allowing brief discussion of longitudinal growth. Most of the subarticular bone formed columns of longitunally oriented trabeculae that are preserved throughout much of the epiphyseal region. The well developed articular surface of the femoral head bears a remarkably thin (~50 microns) layer of calcified cartilage, further supporting that longitudinal growth was nearing completion but had probably not fully ceased. There is no evidence of a secondary ossification center.

Fibula—The fibula (Fig. 9G) is a long, thin bone that is subcirular in section at midshaft and has a bone wall of moderate thickness (*RBT*, 25%; *K*, 0.53). The marrow cavity is lined by smooth endosteal lamellar bone and there are few resorption cavities formed in the perimedullary

PeerJ Reviewing Manuscript

region. The cortex is composed of modestly vascularized FLB having a woven- and parallel-fibered interstitial ECM and numerous small primary osteons (%*CV*, 2.3; mean *POD*, 35 μm). The osteons are almost exclusively longitudinal but with very few reticular anastomoses. The bone maintains a relatively disorganized appearance all the way to the subperiosteal region, with abundant woven-fibered texture and globular osteocyte lacunae. There are no growth marks apparent in the cortex and no EFS.

PeerJ Reviewing Manuscript

Scaloposauridae

Scaloposaurus constrictus

(Fig. 10)

General—SAM-PK-K4638 (humerus), from Vegtlager 801, Wagendriftdam (Lower Triassic, *Lystrosaurus* AZ).

Humerus—A single humerus was available for sectioning. However, poor preservation and slight crushing have distorted aspects of the specimen's cross-sectional shape. The shaft is short but slender, and bears a subcircular cross-section as in other baurioids. The bone wall appears to have been relatively thin, with a large marrow cavity having a few trabeculae as in other baurioids. The trabeculae were formed around the perimedullary region but tended to be localized toward the deltopectoral crest. There appears to have been some endosteal erosion and none of the internal endochondral bone (as reported above in small *Ictidosuchoides*) is retained despite the small size of the individual. The cortex was formed intramembranously by subperiosteally deposited primary bone. The overall tissue texture is fibrolamellar, having a woven-fibered interstitial ECM that incorporated primary osteons. The osteons are relatively

small and longitudinally oriented with a few reticular canals. The overall degree of vascularization is somewhat moderate (%*CV*, 6.6; mean *POD*, 62 μm). Growth marks are absent from the inner cortex, although the texture of the interstitial ECM became more parallel-fibered to lamellar in the outermost cortex with a subperiosteal collar of lamellar bone (~30-40 μm in thickness). Although osteocyte lacunae are generally large, globular and highly concentrated through much of the cortex, they take on an abrupt lenticular appearance and more ordered arrangement within the outer collar of lamellar bone. Although the subperiosteal structure indicates deceleration of growth prior to death, it does not exhibit characteristics of an EFS. Moreover, the full extent of this zone around the periphery of the bone is uncertain due to imperfect preservation and loss of some subperiosteal bone during preparation. Secondary osteons were absent.

PeerJ Reviewing Manuscript

Bauriidae

Microgomphodon oligocynus

(Fig. 11)

General—NMQR 3189 (humerus, femur, tibia, fibula), from Eerstegeluk 131, Bethlehem (Middle Triassic, *Cynognathus* AZ). King (1996) described the morphology of the studied specimen. It consists of a small, disarticulated skeleton preserved within a burrow. In general the limb bones are relatively slender with thin bone walls, bearing large, open marrow cavities as in other baurioids. The cortex consists of FLB with longitudinal, radial, and circular (laminar) primary osteons. Absence of cyclic growth rings indicates fast, sustained growth in the individual. There are no secondary osteons in any of the studied elements.

PeerJ Reviewing Manuscript

Humerus—The humerus (Fig. 11A) has a long, slender shaft with a subcircular cross-section. The bone wall is fairly thin as in other baurioids (*RBT*, 21%; *K*, 0.61) and borders a wide, open marrow cavity that is unobstructed by trabecular structures. A few trabeculae are present in the perimedullary region of the proximal shaft near the deltopectoral crest. The cortex is formed by FLB with a woven- and parallel-fibered matrix and longitudinal and reticular primary osteons (with localized circular canals and abundant parallel-fibered bone along the ventral cortical wall). Osteocyte lacunae are abundant, globular in shape and haphazardly arranged throughout the entire cortex. The cortex is moderately well-vascularized (%*CV*, 8.8; mean *POD*, 43 μm). Growth marks were apparently absent and there is no EFS.

Femur—The histological profile of the femur midshaft (Fig. 11B, C) somewhat resembles that of the humerus, bearing a similarly thin wall (*RBT*, 18%; *K*, 0.61). The marrow cavity is wide, circular and unobstructed by trabeculae, with an abrupt transition to the cortex. There are few resorption cavities along the perimedullary margins. Unlike the humerus, the entire cortex is composed of reticular FLB. The interstitial ECM is predominantly woven-fibered, being disorganized with high concentrations of globular osteocyte lacunae as in the humerus. The reticular primary osteons are densely distributed all the way to the subperiosteal region. Overall, the cortex exhibits moderate vascularization (%*CV*, 6.1; mean *POD*, 44 μm). No growth marks are preserved and there is no EFS.

Tibia—The tibia (Fig. 11D) is somewhat mediolaterally compressed in section and records an irregular transition between the marrow cavity and the cortex at the midshaft. The bone wall is of moderate thickness (*RBT*, 24%; *K*, 0.51), thicker than that of the propodial elements. There are some coarse trabecular structures and a few large resorption cavities along the perimedullary margins. Like the femur, the cortex is largely formed by FLB, although the

primary osteons bear a predominantly longitudinal orientation (with occasional reticular anastomoses). The globular osteocytes were densely-packed around the primary osteons, which were in turn well-concentrated throughout the cortex (%*CV*, 8.0; mean *POD*, 41 μm). No growth marks are preserved and there is no EFS.

Fibula—The fibula (Fig. 11E) is a long, slender bone with an oval midshaft cross-section. The bone wall is somewhat thicker than in the other studied elements (*RBT*, 29%; *K*, 0.39), and the transition to the cortex is relatively abrupt. There were no resorption cavities along the perimedullary regions. Much of the inner cortex bears large, densely packed osteocyte lacunae within a woven-fibered bone matrix. The overall tissue composition is fibrolamellar with longitudinal and occasional radial primary osteons (the latter being most obvious along the posterior region of the bone). The anterior region of the bone bears obliquely-oriented Sharpey's fibers. The overall vascularization is fairly modest (%*CV*, 4.2; mean *POD*, 32 μm). Growth marks are not observed and there is no EFS.

Quantitative Results

Pearson's Product-Moment Correlation and Independent Contrasts

Results of raw and phylogeny-corrected correlation tests are presented in Table 2. Correlation tests on raw data found that vascular growth proxies were strongly positively correlated with the natural log of midshaft cross-sectional area, underscoring greater overall tissue vascularity in large bones from larger taxa (e.g., *Lycosuchus*, scylacosaurids, *Moschorhinus*) (Fig. 12; Table 2). Both %*CV* and *POD* also exhibited a strong positive correlation with each other, indicating that %*CV* and *POD* represent equivalent proxies for understanding relationships between bone tissue vascularization and growth across the

PeerJ Reviewing Manuscript

PeerJ Reviewing Manuscript

therocephalian clade. Whereas these growth proxies shared a consistent positive relationship with size for all data partitions, putative associations between robusticity and size were less clear. Correlation tests on raw size data and *RBT* were non-significant. Likewise, correlation tests on raw vascular growth proxies and *RBT* either yielded non-significant *p*-values or, in the case of the propodial-only data partition, had low correlation coefficients with only a weakly positive association. This result is likely due to the fact that even some small-bodied taxa exhibited unexpectedly thick bone walls, as in the case of the hofmeyriids *Hofmeyria* and *Mirotenthes*. Bone wall thickness correlates poorly with size and growth proxies, suggesting that size and rate of growth may have had limited influence over bone robusticity as compared to other aspects of organismal biology such as mechanical regime (e.g., locomotor behavior, stance or gait; Currey & Alexander, 1985) and ecology or habitat preference (e.g., burrowing, semi-aquatic/aquatic; Wall, 1983; Laurin, Girondot & Loth, 2004; Germain and Laurin, 2005).

Phylogeny-independent contrasts—Results of phylogeny-corrected correlations further indicated a strong relationship between size and histomorphology (but not with limb bone robusticity) (Table 2). Evolutionary decreases in cross-sectional area of limb bones were generally associated with decreases in average %*CV* and *POD*. Eutherocephalians and particularly baurioids demonstrated a noteworthy pattern in which reconstructed ancestor-descendant size reductions of Late Permian and Triassic lineages were associated with decreases in the average level of tissue vascularization. Patterns in limb bone robusticity were less clear. As in the analyses of the raw data, phylogeny-corrected correlations between *RBT* and size or growth proxies were non-significant.

PeerJ Reviewing Manuscript

Discussion

General Histological Patterns

Limb bone cortices in studied therocephalians were generally formed by FLB with varying degrees of vascularization. In Permian therocephalians, multiple growth zones were frequently present, demarcated by cyclic growth marks indicative of periodic cessations of growth as in other Permian therapsids (Ray et al., 2004, 2012; Botha-Brink and Angielczyk, 2010; Botha-Brink et al., 2012). Some small-bodied taxa tended to incorporate more parallel-fibered bone or showed evidence of increased parallel-fibered and lamellar bone deposition with less vasculature toward the outer cortex, indicative of growth attenuation and attainment of somatic maturity (Margerie, Cubo & Castanet, 2002). Fewer taxa demonstrated an EFS-like structure in the outer cortex (*Mirotenthes* being a notable exception). Systematic cortical remodeling by Haversian bone formation was rare and only a few sparse secondary osteons were identified in some scylacosaurian taxa [e.g., an indeterminate scylacosaurid and *Moschorhinus*), contrary to reports of extensive skeletal remodeling suggested by Chinsamy-Turan and Ray (2012: p. 203)]. As in dicynodonts and other therapsids in which histology is well known, most basal therocephalians and eutherocephalians also exhibited remarkably thick bone walls (~20-35% *RBT* in forelimb elements of lycosuchids, scylacosaurids, and akidnognathids; ~40% in forelimbs of hofmeyriids). This condition, however, was lost in baurioids, which were instead characterized by a much thinner cortical bone wall (< 25% in the forelimb and propodials) and longer, more gracile limb bones.

Size, robusticity, and vascular growth proxies—Biologically meaningful associations are detectable in therocephalian histology, as in some other therapsid groups. For example,

vascular growth proxies were strongly positively correlated with size as larger-bodied species typically exhibited greater overall tissue vascularity (e.g., *Lycosuchus*, scylacosaurids, *Moschorhinus*). Previous tests incorporating a large histologic sample of dicynodonts and other therapsids found similar correlations between raw vascular growth proxies and size (estimated from skull lengths), although tests on a subset of dicynodonts were only marginally significant and non-significant when independent contrasts were evaluated (Botha-Brink and Angielczyk, 2010). The new data agree with these earlier results by large measure. However, the present analysis found a strongly positive correlation between size and both vascular growth proxies (%*CV* and *POD*) even when corrected for phylogeny. Prior analyses implementing phylogeny-independent contrasts on dicynodonts were unable to identify similar patterns, despite a significant correlation between the raw data (Botha-Brink and Angielczyk, 2010). Improved statistical results in this study are a likely consequence of sampling bones of particular types separately (rather than averaging vascularity across all bones) and using cross-sectional measurements from sampled bones as a size proxy (rather than skull lengths from specimens that were not sampled histologically). Tests on raw cortical thickness (*RBT*) in dicynodonts also showed no clear association with size or degree of vascularization as in the present study, even though a positive association with size was discovered when corrected for phylogeny. No correlation was observed between bone robusticity (*RBT*) and size or degree of vascularization in therocephalians (raw or phylogeny-corrected), suggesting that bone robusticity is not necessarily tied directly to growth (perhaps being constrained by ecology, habitat, or mechanical regimen in different groups of therocephalians). Similarly, initial data on the genus *Moschorhinus* indicated that overall bone compactness was related to the thickness of the bone wall, but was independent of growth and degree of vascularity (Huttenlocker and Botha-Brink, 2013).

PeerJ Reviewing Manuscript

PeerJ Reviewing Manuscript

Phylogenetic Patterns

Previous interpretations of growth patterns in early therocephalians were based on limited information from incomplete specimens (Ricqlès, 1969; Ray, Botha & Chinsamy, 2004; Chinsamy-Turan and Ray, 2012). Additional specimens described here suggest that at least some large-bodied predators from the Middle Permian, including *Lycosuchus* and some scylacosaurids, exhibited subplexiform FLB in propodial elements. Some of the larger-bodied predators in the sample also showed the highest degree of cortical vascularization. This is remarkable, as subplexiform FLB is one of the most rapidly deposited tissue-types in archosaurian and mammalian limb bones, and similarly vascularized bone in birds and mammals forms periosteally at a rate often greater than 15 µm/day (Castanet et al., 2000; Margerie, Cubo & Castanet, 2002; Cubo et al., 2012). It is noteworthy that the subplexiform tissue complex, present in *Lycosuchus* and scylacosaurids, represents the prototype upon which earlier workers first described FLB [see Stein and Prondvai (2013) for a review]. This subplexiform condition is conspicuously lacking in the whaitsiid *Theriognathus* (Fig. 13) and some later eutherocephalians. Consequently, the evolutionary scenario suggested by Ricqlès (1969) and critically re-examined by Chinsamy-Turan and Ray (2012) should be revised: basal therocephalians exhibited highly vascularized FLB and grew relatively rapidly over many growing seasons but with frequent interuptions, in contrast to some later eutherocephalians (with the exception of the akidnognathid *Moschorhinus,* which maintained relatively fast growth).

Moreover, elevated vascularity and rapid growth may be a characteristic of larger bodied taxa, an interpretation that is supported by observations in other large predatory theriodonts such as the cynodont *Cynognathus* and some large gorgonopsians (Botha-Brink, Abdala & Chinsamy-Turan, 2012; Chinsamy-Turan and Ray, 2012). Importantly, evolutionary decreases in body size

during the Permian were associated with decreases in overall degree of skeletal vascularization. Both hofmeyriids and *Theriognathus* (in spite of its substantial size) showed modest cortical vascularity and smaller mean primary osteon diameters than in basal lycosuchids, scylacosaurids or akidnognathids, but the baurioids (which are deeply nested in the tree and generally smaller-bodied) had the least vascularized bone tissue (Fig. 14). These clade-level patterns suggest that reductions in body size of some Late Permian eutherocephalians were coupled with decreased rates of skeletal apposition leading up to the end-Permian extinction, particularly in the baurioid lineage.

Growth and the End-Permian Extinction

The end-Permian extinction was associated with evidence of temporary body size reductions, restricted primarily to faunas of the earliest Triassic (Induan). Such geologically abrupt size shifts have been documented previously based on invertebrate burrows, foraminifera, brachiopods, gastropods, bivalves, conodonts, and fish (Twitchett and Barras, 2004; Payne, 2005; Twitchett, 2007; Luo et al., 2008; Mutter and Neuman, 2009; Metcalfe, Twitchett & Price-Lloyd, 2011; Song, Tong & Chen, 2011; Rego et al., 2012). Nevertheless, questions remain regarding the evolution of growth patterns and their underlying influence on size shifts (Twitchett, 2007; Harries and Knorr, 2009). For example, organisms may have experienced slower overall growth rates in response to more limited resources or poor environmental conditions. Growth mark analyses on marine brachiopod shells (i.e., '*Lingula'*) have indicated slow growth rates with frequent interuptions to growth in earliest Triassic shells (Metcalfe, Twitchett & Price-Lloyd, 2011). The authors attributed their results to suboptimal environmental conditions, including episodes of benthic hypoxia, hypercapnia, ocean acidification, and/or disruptions to primary productivity. Such environmental factors would place strong

PeerJ Reviewing Manuscript

physiological limits on shell formation. However, identifications of lingulid specimens were tenuous given conservatism in external morphology of the group, and growth marks were only studied in shells from Triassic survival and recovery faunas without being compared to Permian specimens. Alternatively, surviving lineages could have exhibited heterochronic shifts shortening time to maturity (e.g., progenesis) and thus rapid, sustained growth over a brief growth period. Progenesis is a classic example of an *r*-selection strategy in perturbed or unstable environments (Gould, 1977) and has been identified as a potential mechanism of some Lilliput patterns (Harries, Kauffman & Hansen, 1996). Finally, if shifts in body size distributions were influenced primarily by differential extinction of large- versus small-bodied forms, then there may have been no resulting changes in growth patterns at all (that is to say, changes in growth dynamics are not necessary to explain post-extinction body size distributions).

Growth patterns in Permo-Triassic therapsids compared—New data on growth patterns in nonmammalian therapsids, as well as other Permo-Triassic tetrapods, offer the potential to further evaluate patterns of selectivity during mass extinctions (Botha-Brink and Angielczyk, 2010; Botha-Brink and Smith, 2012). Bone histology has been studied in numerous genera of Permian and Triassic dicynodont therapsids (Chinsamy and Rubidge, 1993; Ray, Botha & Chinsamy, 2004; Ray, Bandyopadhyay & Bhawal, 2009; Ray, Botha-Brink & Chinsamy-Turan, 2012) and recent progress in dicynodont paleobiology has permitted evolutionary investigations of their growth patterns (Botha-Brink and Angielczyk, 2010). Increased rates of skeletal growth originated relatively early, either within or prior to the divergence of bidentalian dicynodonts (e.g., *Dicynodon*, *Lystrosaurus*) by the early-Late Permian. Medium-to-large Late Permian dicynodonts continued to show patterns of increased cortical vascularity, especially within the Permo-Triassic boundary-crossing genus *Lystrosaurus*, which demonstrated some of

PeerJ Reviewing Manuscript

the highest levels of tissue vascularity (~20%). Triassic specimens of *Lystrosaurus* showed relatively higher vascularity and fewer growth marks. In the therocephalian *Moschorhinus*, the only large therapsid predator to cross the Permian-Triassic boundary, within-lineage size reductions were associated with the maintenance of rapid but attenuating growth over a short period (Huttenlocker and Botha-Brink, 2013). This pattern suggests that *Moschorhinus* may have been under selection for reaching its adult size relatively more quickly than in other Permian therocephalians. Notably, *Moschorhinus* exhibited comparably high levels of tissue vascularity as *Lystrosaurus* during the Triassic (~20-25%).

Whereas anecdotal evidence in *Lystrosaurus* and *Moschorhinus* is suggestive of within-lineage heterochronic shifts, clade-level patterns introduce a more complex explanation for observed body size reductions in therocephalians. In particular, body size reductions occurred early during the evolution of eutherocephalians and were associated with a lesser degree of cortical vascularity in medium-to-small-bodied Permian forms (e.g., hofmeyriids and especially baurioids). The two major subclades of therocephalians that persisted into the earliest Triassic, Akidnognathidae and Baurioidea, revealed distinctly different growth patterns from each other as interpreted through their tissue texture and degree of vascularity. Their histology suggests a bimodality of life history strategies in earliest Triassic therocephalians: small-to-medium akidnognathids with well-vascularized (fast-growing) bone and smaller-bodied baurioids with less vascularized (slower-growing) bone. However, both groups shared a reduced number of growth marks compared to their Permian relatives in addition to their generally smaller sizes. This nuance is not evident from the quantitative analysis based on vascular proxies of growth rate alone, but is evident from growth mark counts in surveyed specimens. Permian theriodonts that have been sampled histologically, including some gorgonopsians, the cynodont

PeerJ Reviewing Manuscript

PeerJ Reviewing Manuscript

Procynosuchus, basal therocephalians, Permian (but not Triassic) specimens of *Moschorhinus*, hofmeyriids, and *Theriognathus*, typically showed evidence of prolonged, multi-year growth often to larger body sizes, a pattern that is not represented in earliest Triassic therapsids sampled to date (Botha-Brink and Angielczyk, 2010; Botha-Brink, Abdala & Chinsamy, 2012).

Microstructural and macrostructural evolution during the Permian-Triassic transition—The present discussion of associations between micro- and macrostructure provides a more functional and wholistic context for the evolution of histological features in Permian and Triassic therocephalians. However, it is important to note that the patterns discussed here have not been evaluated quantitatively and therefore merit future investigation. Recent large-scale phylogenetic studies in other therapsids have addressed how life history and functional morphology might have contributed to the success of some groups during the Late Permian and Triassic (e.g., bidentalian dicynodonts). For example, the degree of development of the secondary palate has been linked anecdotally to new environmental conditions with the onset of the Early Triassic, particularly a dramatic decline in atmospheric pO_2 from the Late Permian and continuing through the Middle and Late Triassic (Retallack, 2003). However, a rigorous collections-based study found no difference between secondary palate length in Permian and Triassic dicynodonts when corrected for size and phylogeny (Angielczyk and Walsh, 2008). Similarly, a bony secondary palate can be found in a number of therocephalian subgroups, both in the Permian and Triassic, and Triassic therocephalian faunas consisted of species both with (e.g., baurioids) and without (e.g., akidnognathids) a secondary palate. No clear association with global hypoxia and respiratory efficiency can be made based on this character, and, as a result, other factors may have been more important in maintaining and shaping the evolution of the secondary palate (e.g., feeding mechanics; Thomason and Russell, 1986).

PeerJ Reviewing Manuscript

Similar studies addressing the possible effects of hypoxia on cortical tissue vascularity have found few differences between Permian and Triassic therapsids, instead demonstrating that highly vascularized tissues with enlarged canals evolved early in bidentalian dicynodonts (Botha-Brink and Angielczyk, 2010). In therocephalians, variation in the degree of vascularization of limb cortices is best explained by size variation observed across clades. Most smaller-bodied groups exhibited less vascularized limb bone cortices, a character that evolved relatively early in the evolutionary history of eutherocephalians and held over in some small Triassic taxa. The smallest Triassic forms, derived bauroids, typically had lighter, more gracile skeletons with an open medullary cavity, thinner bone walls, and few to no growth marks. In addition to longer, more slender limb bones, they also had an elongate hind foot with a calcaneal tuber on the heel, maxillary bridge forming a bony secondary palate (discussed above), increasingly specialized multi-cusped teeth, and often lacked a parietal foramen (or reduced the pineal body altogether as in *Tetracynodon*; Sigurdsen et al., 2012). The selective value of maintaining a parietal eye for temperature regulation and modulating melatonin production may have been diminished in some small, nocturnal or crepuscular baurioid therocephalians, or in short-lived animals less dependent on seasonal cues in photoperiodicity (Roth, Roth & Hotton, 1986). The latter scenario is consistent with the lack of cyclic bone deposition and paucity of growth marks in small Triassic baurioids (although one genus, *Scaloposaurus*, is distinguished from other small Triassic baurioids in its retention of the parietal foramen and pineal body).

Conclusion

A survey of histological patterns in therocephalians found that limb bone cortices composed of thick deposits of FLB with cyclic growth marks were widespread in early

PeerJ Reviewing Manuscript

therocephalians, but evolutionary decreases in adult body sizes of some clades were associated with reductions in cortical vascularity and skeletal growth leading up to the end-Permian mass extinction. In Permo-Triassic therocephalians, a pattern of multi-year growth to large body size that was common in the Permian was selected against in the earliest Triassic. This conclusion is supported by (1) ecological removal of large-bodied taxa having prolonged, multi-year growth patterns; (2) cladistically inferred survival of small-bodied taxa with modest skeletal apposition rates, but truncated growth durations (i.e., baurioids); and (3) within-lineage shifts in growth patterns observed in boundary-crossing genera in the Karoo (i.e., *Lystrosaurus* and *Moschorhinus*). A synergistic combination of local within-lineage effects and differential extinction patterns strongly influenced Triassic Lilliput faunas, weakening the hypothesized role of rapid adaptive evolution of new small-bodied forms. Similar within-lineage size decreases and size selective extinctions contributed strongly to Lilliput patterns in marine gastropods, foraminifera, and brachiopods, although all three mechanisms have been invoked to explain Early Triassic foraminifera size distributions globally (Payne, 2005; Metcalfe, Twitchett & Price-Lloyd, 2011; Song, Tong & Chen, 2011; Rego et al., 2012). Contrary to the present results, growth mark analyses on lingulid brachiopods are suggestive of different physical factors influencing skeletal growth in marine benthos (due to slowed, but prolonged shell secretion over many years) (Metcalfe, Twitchett & Price-Lloyd, 2011). More skeletochronologic and phylogenetic data are needed, however, to understand the generality of these patterns among Permo-Triassic Lilliput taxa in marine and terrestrial realms.

Although some effects on size and growth are observable in Triassic therocephalians (and perhaps therapsids more generally), it is important to note that much of the diversity observed in the earliest Triassic *Lystrosaurus* Assemblage Zone of the Karoo originated during the Late

PeerJ Reviewing Manuscript

Permian, and that variation in body sizes and growth patterns during the Late Permian was supplanted by increased bimodality in the Early Triassic *Lystrosaurus* AZ: small-to-medium, fast-growing akidnognathids and the still smaller, slower-growing baurioids. Small size and short growth duration were dominant life history strategies of Early Triassic therocephalians in the Karoo, and reductions in size were typically associated with lesser tissue vascularity and growth rates across but not within taxa. Furthermore, although these strategies were apparently common in the post-extinction environment, their success was temporary. Low rates of origination in therocephalians during this time, coupled with small sizes and reduced niche occupation may have afforded the opportunity for more marginalized groups to diversify (e.g., cynodonts and archosauromorphs). Future applications of phylogenetic comparative methods to studies of body size and growth during the Permo-Triassic will enhance our understanding of interplay between macroevolution and extinctions, and will identify areas of phylogeny that correspond to shifts in trait evolution that conferred success on lineages.

Acknowledgments

AKH thanks S. Herring, E. Nesbitt, C. Sidor, and G. Wilson for providing helpful suggestions on the project. F. Abdala and B. Rubidge (BP), E. Butler (NMQR), E. De Kock and J. Neveling (CGS), P. Holroyd (UCMP), and S. Kaal and R. Smith (SAM) are acknowledged for specimen access. F. Abdala and K. Angielczyk offered additional insights into body size evolution and growth, as well as therapsid diversity patterns during the end-Permian extinction. Digital image processing and some histologic preparation performed by J. Lungmus (University of Washington). Funding to AKH was provided by the National Science Foundation Doctoral Dissertation Improvement Grant Program (1209018), Evolving Earth Foundation, University of

Washington Department of Biology WRF-Hall Fellowship, Burke Museum of Natural History and Culture Vertebrate Paleontology Fellowship, and the Society of Vertebrate Paleontology Richard Estes Memorial Grant. Funding to JB-B was provided by the National Research Foundation (Early Triassic Recovery Project, NRF-65244), Republic of South Africa. The funders had no role in study design, data collection and analysis, or preparation of the manuscript.

PeerJ Reviewing Manuscript

References

Abdala F, Rubidge BS, van den Heever J. 2008. The oldest therocephalians (Therapsida, Eutheriodontia) and the early diversification of Therapsida. *Palaeontology* 51:1011–1024.

Angielczyk KD, Walsh ML. 2008. Patterns in the evolution of nares size and secondary palate length in anomodont therapsids (Synapsida): implications for hypoxia as a cause of end-Permian tetrapod extinctions. *Journal of Paleontology* 82:528-542.

Botha J. 2003. Biological aspects of the Permian dicynodont *Oudenodon* (Therapsida:Dicynodontia) deduced from bone histology and cross-sectional geometry. *Palaeontologia Africana* 39:37–44.

Botha J, Angielczyk K. 2007. An integrative approach to distinguishing the Late Permian dicynodont species *Oudenodon baini* and *Tropidostoma microtrema* (Therapsida: Anomodontia). *Palaeontology* 50:1175–1209.

Botha J, Chinsamy A. 2000. Growth patterns deduced from the histology of the cynodonts *Diademodon* and *Cynognathus*. *Journal of Vertebrate Paleontology* 20:705–711.

Botha J, Chinsamy A. 2004. Growth and lifestyle adaptations of the Triassic non-mammalian cynodont *Trirachodon*. *Acta Palaeontologica Polonica* 49:619–627.

Botha J, Chinsamy A. 2005. Growth patterns of *Thrinaxodon*, a non-mammalian cynodont from the Early Triassic of South Africa. *Palaeontology* 48:385–394.

Botha J, Smith RMH. 2006. Rapid vertebrate recuperation in the Karoo Basin of South Africa following the end-Permian extinction. *Journal of African Earth Sciences* 45:502–514.

Botha-Brink J & al. 2012. The radiation and osteohistology of nonmammaliaform cynodonts. *Forerunners of Mammals: Radiation, Histology, Biology,* Indiana University Press, Bloomington, ed Chinsamy-Turan A, pp. 223–246.

Botha-Brink J, Angielczyk K. 2010. Do extraordinarily high growth rates in Permo-Triassic dicynodonts (Therapsida, Anomodontia) explain their success before and after the end-Permian extinction? *Zoological Journal of the Linnean Society* 160:341–365.

Botha-Brink J, Modesto SP. 2011. A new skeleton of the therocephalian synapsid *Olivierosuchus parringtoni* from the Lower Triassic South African Karoo Basin. *Palaeontology* 54:591–606.

Botha-Brink J, Smith RMH. 2012. Osteohistology of the Triassic archosauromorphs *Prolacerta*, *Proterosuchus*, *Euparkeria*, and *Erythrosuchus* from the Karoo Basin of South Africa. *Journal of Vertebrate Paleontology* 31:1238–1254.

Buffrénil V de & al. 2007. Bone vascular supply in monitor lizards (Squamata: Varanidae): implications of size, growth, and phylogeny. *Journal of Morphology* 269:533–543.

Calder WA III. 1984. *Size, Function, and Life History*. Harvard University Press, Cambridge: 431 pp.

Case TJ. 1978. On the evolution and adaptive significance of postnatal growth rates in the terrestrial vertebrates. *The Quarterly Review of Biology* 53:243–282.

PeerJ Reviewing Manuscript

Castanet J & al. 2000. Periosteal bone growth rates in extant ratites (ostrich and emu): implications for assessing growth in dinosaurs. *Comptes Rendus de l'Académie des Sciences de Paris***,** *Science de la Vie* 323:543–550.

Chinsamy A. 1993. Bone histology and growth trajectory of the prosauropod dinosaur *Massospondylus carinatus* Owen. *Modern Geology* 18:319–329.

Chinsamy A, Abdala F. 2008. Paleobiological implications of the bone microstructure of South American traversodontids (Therapsida: Cynodontia). *South African Journal of Science* 104:225–230.

Chinsamy A, Hurum J. 2006. Bone microstructure and growth patterns of early mammals. *Acta Palaeontologica Polonica* 51:325–338.

Chinsamy A, Raath M. 1992. Preparation of fossil bone for histological examination. *Palaeontologia Africana* 29:39–44.

Chinsamy A, Rubidge BS. 1993. Dicynodont (Therapsida) bone histology: Phylogenetic and physiological implications. *Palaeontologia Africana* 30:97–102.

Chinsamy-Turan A. 2012. *Forerunners of Mammals: Radiation, Histology, Biology.* Indiana University Press, Bloomington.

Chinsamy-Turan A, Ray S. 2012. Bone histology of some therocephalians and gorgonopsians, and evidence of bone degradation by fungi. *Forerunners of Mammals: Radiation, Histology, Biology,* Indiana University Press, Bloomington, ed Chinsamy-Turan A, pp. 199–221.

Cubo, J & al. 2012. Paleohistological estimation of bone growth rate in extinct archosaurs. *Paleobiology* 38:335–349.

Currey JD. 1987. The evolution of the mechanical properties of amniote bone. *Journal of Biomechanics* 20:1035–1044.

PeerJ Reviewing Manuscript

Currey JD. 2002. *Bones: Structure and Mechanics, 2nd ed.* Princeton University Press, Princeton, N.J.

Currey JD, Alexander RMcN. 1985. The thickness of the walls of tubular bones. *Journal of Zoology* 206:453–468.

Díaz-Uriarte R, Garland T. 1996. Testing hypotheses of correlated evolution using phylogenetically independent contrasts: sensitivity to deviations from Brownian motion. *Systematic Biology* 45:27–47.

Enlow DH. 1969. The bone of reptiles. *Biology of the Reptilia, Volume 1: Morphology A*, Academic Press, London, eds Gans C, Bellairs A, & Parsons T, pp. 45-77.

Enlow DH, Brown SO. 1957. A comparative histological study of fossil and Recent bone tissues, Part II. *Texas Journal of Science* 9:186–214.

Erickson G & al. 2004. Gigantism and comparative life-history parameters of tyrannosaurid dinosaurs. *Nature* 430:772–775.

Felsenstein J. 1985. Phylogenies and the comparative method. *American Naturalist* 125:1–15.

Fourie H, Rubidge BS. 2007. The postcranial skeletal anatomy of the therocephalian *Regisaurus* (Therapsida: Regisauridae) and its utilization for biostratigraphic correlation. *Palaeontologia Africana* 42:1–16.

Fourie H, Rubidge BS. 2009. The postcranial skeleton of the basal therocephalian *Glanosuchus macrops* (Scylacosauridae) and comparison of morphological and phylogenetic trends amongst the Theriodontia. *Palaeontologia Africana* 44:27–39.

Garland T & al. 2005. Phylogenetic approaches in comparative physiology. *Journal of Experimental Biology* 208:3015–3035.

PeerJ Reviewing Manuscript

Germain D, Laurin M. 2005. Microanatomy of the radius and lifestyle in amniotes (Vertebrata, Tetrapoda). *Zoologica Scripta* 34:335–350.

Gould SJ. 1977. *Ontogeny and Phylogeny*. Belknap Press of Harvard University Press, Cambridge.

Green JL & al. 2010. Limb bone histology and growth in *Placerias hesternus* (Therapsida: Anomodontia) from the Upper Triassic of North America. *Palaeontology* 53:347–364.

Harries PJ, Kauffman EG, Hansen TA. 1996. Models of biotic survival following mass extinction. *Biotic Recovery from Mass Extinction Events. Geological Society of London Special Publication* 102, ed Hart MB, pp. 41–60.

Harries PJ, Knorr PO. 2009. What does the 'Lilliput Effect' mean? *Palaeogeography, Palaeoclimatology, and Palaeoecology* 284:4–10.

Horner J & al. 2001. Comparative osteohistology of some embryonic and perinatal archosaurs: developmental and behavioral implications for dinosaurs. *Paleobiology* 27:39–58.

Huttenlocker AK. 2009. An investigation into the cladistic relationships and monophyly of therocephalian therapsids (Amniota: Synapsida). *Zoological Journal of the Linnean Society* 157:865–891.

Huttenlocker AK. In review. Body size reductions in nonmammalian eutheriodonts (Amniota, Therapsida) before and after the end-Permian mass extinction. *PLOS:ONE*.

Huttenlocker AK, Botha-Brink J. 2013. Body size and growth patterns in the therocephalian *Moschorhinus kitchingi* (Therapsida: Eutheriodontia) before and after the end-Permian extinction in South Africa. *Paleobiology* 39:253–277.

Huttenlocker AK & al. 2011. Comparative osteohistology of hyperelongate neural spines in the Edaphosauridae (Amniota: Synapsida). *Palaeontology* 54:573–590.

PeerJ Reviewing Manuscript

Huttenlocker AK, Rega E. 2012. The paleobiology and bone microstructure of pelycosaurian-grade synapsids. *Forerunners of Mammals: Radiation, Histology, Biology,* Indiana University Press, Bloomington, ed Chinsamy-Turan A, pp. 90–119.

Huttenlocker AK & al. 2010. Comparative anatomy and osteohistology of hyperelongate neural spines in the sphenacodontids *Sphenacodon* and *Dimetrodon* (Amniota: Synapsida). *Journal of Morphology* 271:1407–1421.

Huttenlocker AK & al. 2011. A new specimen of *Promoschorhynchus* (Therapsida: Therocephalia: Akidnognathidae) from the Lower Triassic of South Africa and its implications for theriodont survivorship across the Permo-Triassic boundary. *Journal of Vertebrate Paleontology* 31:405–421.

Jasinoski SC & al. 2010. Functional implications of dicynodont cranial suture morphology. *Journal of Morphology* 271:705–728.

Kemp TS. 1972a. Whaitsiid Therocephalia and the origin of cynodonts. *Philosophical Transactions of the Royal Society of London: Series B* 264:1-54.

Kemp TS. 1972b. The jaw articulation and musculature of the whaitsiid Therocephalia. *Studies in Vertebrate Evolution,* Winchester Press, New York, eds Joysey KA & Kemp TS, pp. 213-230.

Kemp TS. 1978. Stance and gait in the hindlimb of a therocephalian mammal-like reptile. *Journal of Zoology* 186:143–161.

Kemp TS. 1986. The skeleton of a baurioid therocephalian therapsid from the Lower Triassic (*Lystrosaurus* Zone) of South Africa. *Journal of Vertebrate Paleontology* 6:215–232.

King GM. 1996. A description of the skeleton of a bauriid therocephalian from the Early Triassic of South Africa. *Annals of the South African Museum* 104:379–393.

PeerJ Reviewing Manuscript

Kitching JW. 1977. The distribution of the Karroo vertebrate fauna. *Bernard Price Institute for Palaeontological Research Memoir 1*. The Natal Witness Ltd.: 131 pp.

Kriloff A & al. 2008. Evolution of bone microanatomy of the tetrapod tibia and its use in paleobiological inference. *Journal of Evolutionary Biology* 21:807–826.

Laurin M & al. 2004. The evolution of long bone microstructure and lifestyle in lissamphibians. *Paleobiology* 30:589–613.

Lee AH. 2007. *Interplay Between Growth and Mechanics in the Evolution of Bone Microstructure in Dinosaurs*. Unpublished Ph.D. dissertation. University of California, Berkeley: 210 pp.

Lee AH & al. 2013. Chapter 8: Analysis of growth rates. *Bone Histology of Fossil Tetrapods: Advancing Methods, Analysis, and Interpretation*, University of California Press, Berkeley, eds Padian K & Lamm E-T, pp. 209–243.

Luo G & al. 2008. Size variation of conodont elements of the *Hindeodus-Isarcicella* clade during the Permian-Triassic transition in South China and its implications for mass extinction. *Palaeogeography, Palaeoclimatology, Palaeoecology* 264:176–187.

Maddison WP, Maddison DR. 2007. Mesquite: a modular system for evolutionary analysis. Version 2.0. http://mesquiteproject.org

Margerie E de & al. 2002. Bone typology and growth rate: testing and quantifying 'Amprino's rule' in the mallard (*Anas platyrhynchos*). *Comptes Rendus Biologies* 325:221–230.

Margerie E de & al. 2004. Assessing a relationship between bone microstructure and growth rate: a fluorescent labeling study in the king penguin chick (*Aptenodytes patagonicus*). *Journal of Experimental Biology* 207:869–879.

PeerJ Reviewing Manuscript

Metcalfe B & al. 2011. Size and growth rate of 'Lilliput' animals in the earliest Triassic. *Palaeogeography, Palaeoclimatology, Palaeoecology* 308:171–180.

Midford PE. 2011. PDAP:PDTREE module for Mesquite (version 1.16). http://mesquiteproject.org/pdap_mesquite/index.html.

Mutter RJ, Neuman AG. 2009. Recovery from the end-Permian extinction event: evidence from "Lilliput *Listracanthus*." *Palaeogeography, Palaeoclimatology, Palaeoecology* 284:22–28.

Nasterlack T & al. 2012. New insights into the biology of the Permian genus *Cistecephalus* (Therapsida, Dicynodontia). *Journal of Vertebrate Paleontology* 32:1396–1410.

Payne JL. 2005. Evolutionary dynamics of gastropod size across the end-Permian extinction and through the Triassic recovery interval. *Paleobiology* 31:269–290.

Peters R. 1983. *The Ecological Implications of Body Size*. Cambridge University Press, Cambridge: 344 pp.

Ray S & al. 2005. *Lystrosaurus murrayi* (Therapsida; Dicynodontia): bone histology, growth and lifestyle adaptations. *Palaeontology* 48:1169–1185.

Ray S & al. 2009. Growth patterns as deduced from bone microstructure of some selected neotherapsids with special emphasis on dicynodonts: Phylogenetic implications. *Palaeoworld* 18:53–66.

Ray S & al. 2010. Chapter 5: Bone histology of a kannemeyriid dicynodont *Wadiasaurus*: palaeobiological implications. *New Aspects of Mesozoic Biodiversity (Lecture Notes in Earth Sciences 132)* Springer, Berlin, ed Bandyopadhyay S, pp. 73–89.

Ray S & al. 2004. Bone histology and growth patterns of some nonmammalian therapsids. *Journal of Vertebrate Paleontology* 24:634–648.

PeerJ Reviewing Manuscript

Ray S & al. 2012. Dicynodont growth dynamics and lifestyle adaptations. *Forerunners of Mammals: Radiation, Histology, Biology,* Indiana University Press, Bloomington, ed Chinsamy-Turan A, pp. 121–146.

Ray S, Chinsamy A. 2004. *Diictodon feliceps* (Therapsida, Dicynodontia): bone histology, growth and biomechanics. *Journal of Vertebrate Paleontology* 24:180–194.

Rego BL & al. 2012. Within- and among-genus components of foraminiferan size evolution during mass extinction, recovery, and background intervals. *Paleobiology* 38:627–643.

Retallack GJ. 2003. Vertebrate extinction across the Permian-Triassic boundary in the Karoo Basin of South Africa. *Bulletin of the Geological Society of America* 115:1133–1152.

Ricqlès A de. 1969. Recherches paléohistologiques sur les os longs des Tétrapodes II—Quelques observations sur la structure des os longs des Thériodontes. *Annales de Paléontologie (Vertébrés)* 55:1–52. [in French]

Ricqlès A de. 1974a. Evolution of endothermy: histological evidence. *Evolutionary Theory* 1:51–80.

Ricqlès A de. 1974b. Recherches paléohistologiques sur les os longs des Tétrapodes IV—Eothériodontes et pélycosaures. *Annales de Paléontologie (Vertébrés)* 60:3–39. [in French]

Ricqlès A de. 1976. On bone histology of fossil and living reptiles, with comments on its functional and evolutionary significance. *Morphology and Biology of Reptiles*, Academic Press, London, eds Bellairs A & Cox CB, pp.123–150.

Roth, JJ & al. 1986. The parietal foramen and eye: their function and fate in therapsids. *The Ecology and Biology of Mammal-like Reptiles*. Smithsonian Institution Press, Washington, D.C., eds Hotton N, MacLean PD, Roth JJ, & Roth EC, pp. 173–184.

PeerJ Reviewing Manuscript

Sigurdsen T. 2006. New features of the snout and orbit of a therocephalian therapsid from South Africa. *Acta Palaeontologica Polonica* 51:63–75.

Sigurdsen T & al. 2012. Reassessment of the morphology and paleobiology of the therocephalian *Tetracynodon darti* (Therapsida), and the phylogenetic relationships of Baurioidea. *Journal of Vertebrate Paleontology* 32:1113–1134.

Smith RMH, Botha J. 2005. The recovery of terrestrial vertebrate diversity in the South African Karoo Basin after the end-Permian extinction. *Comptes Rendus Palevol* 4:623–636.

Song H & al. 2011. Evolutionary dynamics of the Permian-Triassic foraminifer size: Evidence for Lilliput effect in the end-Permian mass extinction and its aftermath. *Palaeogeography, Palaeoclimatology, Palaeoecology* 308:98–110.

Stearns SC. 1992. *The Evolution of Life Histories*. Oxford University Press, Oxford: 249 pp.

Stein K, Prondvai E. 2013. Rethinking the nature of fibrolamellar bone: an integrative biological revision of sauropod plexiform bone formation. *Biological Reviews of the Cambridge Philosophical Society* 2013. doi: 10.1111/brv.12041

Thomason JJ, Russell AP. 1986. Mechanical factors in the evolution of the mammalian secondary palate: a theoretical analysis. *Journal of Morphology* 189:199–213.

Twitchett RJ. 2007. The Lilliput effect in the aftermath of the end-Permian extinction event. *Palaeogeography, Palaeoclimatology, Palaeoecology* 252:132–144.

Twitchett RJ, Barras CG. 2004. Trace fossils in the aftermath of mass extinction events. *The Application of Ichnology to Palaeoenvironmental and Stratigraphic Analysis, Geological Society Special Publications 228*, Geological Society of London, London, ed McIlroy D, pp. 397-418.

PeerJ Reviewing Manuscript

Urbanek A. 1993. Biotic crises in the history of Upper Silurian graptoloids: a paleobiological model. *Historical Biology* 7:29–50.

Wall PW. 1983. The correlation between high limb-bone density and aquatic habitats in recent mammals. *Journal of Paleontology* 57:197–207.

Wilson JW. 1994. Histological techniques. *Vertebrate Paleontological Techniques* Cambridge University Press, New York, ed Leiggi P & May P, pp. 205–234.

PeerJ Reviewing Manuscript

Appendix 1. List of institutional abbreviations.

BP, Evolutionary Studies Institute (previously Bernard Price Institute for Palaeontological Research), University of Witwatersrand, Johannesburg; **CGS**, Council for Geoscience, Pretoria (former Geological Survey field numbers); **NMQR**, National Museum, Bloemfontein; **SAM**, Iziko South African Museum, Cape Town; **UCMP**, University of California Museum of Paleontology, Berkeley.

PeerJ Reviewing Manuscript

PeerJ Reviewing Manuscript

Tables & Figure Captions

Table 1. Specimens, elements, and histomorphometric measurements in studied therocephalians.

	% Largest*	Element	Midshaft cross-sectional area (mm^2)	*RBT* (%)	*K*	Cortical vascularity (%)	Mean POD (µm)
Lycosuchus							
SAM-PK-9084	100%	radius	296.76	16	0.42	10.7[5.5]	101[11]
		ulna	325.40	25	0.38	15.7[2.0]	109[26]
SAM-PK-K9012	--	femur	1276.60	15	0.67	16.9[6.2]	168[17]
Glanosuchus							
BP/1/6228	47%	ulna	57.62	20	0.42	04.9[0.9]	51[13]
Scylacosauridae indet.							
BP/1/5576	--	radius	30.99	19	0.47	10.3[2.2]	68[10]
		ulna	36.63	24	0.53	09.7[4.3]	71[08]
BP/1/5587	--	humerus	169.42	33	0.29	13.3[3.2]	75[08]
		radius	88.26	23	0.46	03.5[0.7]	71[15]
		ulna	120.25	24	0.44	06.0[0.8]	85[07]
CGS R300	--	humerus	308.56	31	0.32	15.9[6.5]	112[13]
SAM-PK-5018	--	humerus	--	--	--	--	--
		radius	--	17	--	--	--
		femur	--	15	--	--	--
		tibia	83.86	24	0.60	10.3[1.5]	55[10]
		fibula	--	--	--	--	--
SAM-PK-11557	--	fibula	49.10	25	0.47	07.0[2.8]	44[07]
Moschorhinus							
NMQR 48	62%	humerus	205.85	30	0.45	16.6[5.0]	--
		radius	48.10	26	0.40	05.2[2.4]	67[18]
		ulna	102.67	27	0.43	04.8[1.3]	67[10]
		femur	263.13	22	0.58	12.8[4.8]	95[13]
NMQR 3939	65%	humerus	212.25	35	0.38	20.1[6.9]	134[36]
		radius	92.77	34	0.31	11.4[2.6]	101[18]
		ulna	101.86	29	0.44	10.1[2.1]	120[27]
		femur	206.82	28	0.44	18.4[6.9]	140[32]
		tibia (l)	103.85	37	0.30	15.5[1.9]	117[17]
		tibia (r)	114.28	31	0.39	15.6[5.8]	119[34]
NMQR 1640a	(84%)	femur	325.70	25	0.50	11.1[4.8]	96[12]
NMQR 1640b	--	tibia	427.87	35	0.39	09.7[2.5]	106[23]
NMQR 3351	91%	femur	488.65	21	0.55	13.6[5.0]	100[22]
NMQR 3684	(95%)	femur	378.12	27	0.53	14.2[4.6]	92[17]
SAM-PK-K118	59%	humerus	161.60	28	0.41	25.5[4.9]	100[17]
		radius	62.80	23	0.54	19.5[3.2]	101[17]
SAM-PK-K9953	59%	femur	155.13	25	0.42	20.9[5.8]	108[15]
UCMP 42787	(67%)	humerus	209.64	35	0.34	19.5[4.0]	107[20]
		radius	83.64	35	0.27	12.4[3.6]	92[18]
		fibula	42.53	32	0.28	10.8[1.9]	58[14]
BP/1/4227	76%	humerus	312.00	33	0.35	12.1[2.9]	100[16]
		radius	103.60	30	0.36	10.9[2.1]	88[10]
		ulna	96.00	26	0.48	08.5[2.0]	91[19]

Table 1. (Continued)

Olivierosuchus							
NMQR 3605	100%	humerus	47.54	36	0.38	09.9[1.8]	99[10]
SAM-PK-K10617	(65%)	femur	23.72	19	0.65	03.4[1.1]	75[10]
Hofmeyria							
BP/1/4404	69%	humerus	12.56	31	0.32	07.5[1.4]	72[11]
		radius (l)	4.80	35	0.26	03.4[1.0]	46[05]
		radius (r)	4.04	40	0.15	04.8[1.9]	47[05]
		ulna (l)	3.63	39	0.22	03.0[0.6]	39[05]
		ulna (r)	4.30	39	0.20	04.7[1.1]	43[08]
Mirotenthes							
SAM-PK-K6511	78%	humerus	17.12	32	0.31	05.4[1.5]	54[07]
		radius	6.28	34	0.33	03.5[1.5]	38[07]
		ulna	5.24	32	0.42	02.0[0.5]	41[07]
		femur	19.40	25	0.42	03.6[0.6]	58[07]
		tibia	11.28	31	0.31	03.1[0.8]	38[06]
		fibula	3.64	32	0.39	03.9[1.1]	32[04]
Theriognathus							
NMQR 3375	38%	femur	43.45	24	0.51	06.2[2.0]	65[10]
BP/1/719	(62%)	femur	140.21	20	0.59	06.8[1.4]	87[11]
Ictidosuchoides							
SAM-PK-K8659	50%	humerus	23.92	22	0.56	07.3[2.0]	45[05]
		radius	10.08	24	0.52	04.2[1.1]	38[05]
		femur	45.64	--	--	--	38[05]
		tibia	28.32	16	0.63	02.8[1.0]	43[08]
		fibula	10.44	22	0.59	03.8[1.5]	40[07]
SAM-PK-K10423	(50%)	femur	34.80	14	0.71	04.7[1.8]	65[08]
		tibia	9.52	23	0.49	04.3[1.5]	39[05]
		fibula	19.60	19	0.47	04.7[1.6]	40[08]
BP/1/75	--	humerus	44.27	19	0.64	11.1[1.4]	52[06]
BP/1/4092	100%	humerus	60.19	22	0.56	10.2[2.1]	60[07]
		radius	39.52	21	0.58	11.1[3.1]	62[08]
		ulna	74.67	26	0.54	08.3[2.1]	52[08]
Tetracynodon							
NMQR 3745	85%	humerus	11.44	22	0.56	8.1[3.2]	36[10]
UCMP 78395	(94%)	humerus	16.48	24	0.49	4.9[1.7]	42[05]
		radius	8.40	27	0.43	1.9[0.5]	42[10]
		ulna	6.12	31	0.33	2.8[1.0]	38[06]
		femur	18.28	17	0.66	5.0[2.5]	39[06]
		tibia	12.48	25	0.48	3.9[0.7]	42[06]
UCMP 78396	(94%)	humerus	16.96	21	0.54	4.7[1.9]	42[12]
		femur	18.16	17	0.62	4.3[1.1]	42[07]
		fibula	5.19	25	0.53	2.3[0.5]	35[06]
Scaloposaurus							
SAM-PK-K4638	67%	humerus	15.34	--	--	06.6[1.6]	62[08]

PeerJ Reviewing Manuscript

Table 1. (Continued)

Microgomphodon							
NMQR 3189	(82%)	humerus	11.04	21	0.61	08.8[2.1]	43[08]
		femur	16.52	18	0.61	06.1[1.6]	44[08]
		tibia	7.86	24	0.51	08.0[3.2]	41[09]
		fibula	3.33	29	0.39	04.2[0.9]	32[04]

*Based on relative basal skull length (BSL). Parentheses indicate estimates for incomplete skulls.

PeerJ Reviewing Manuscript

Table 2. Pearson's product-moment correlation statistics (Pearson's *r* and *p*) for size, robusticity, and vascular growth proxies in therocephalians.

	Propodial-only		Epipodial-only		Pooled	
	r	*p**	*r*	*p*	*r*	*p*
All therocephalians, raw data						
ln midshaft area vs. RBT	0.309	0.109	−0.186	0.267	−0.126	0.301
ln midshaft area vs. %CV	**0.744**	**<0.001**	**0.714**	**<0.001**	**0.746**	**<0.001**
ln midshaft area vs. POD	**0.853**	**<0.001**	**0.847**	**<0.001**	**0.850**	**<0.001**
RBT vs. %CV	**0.452**	**0.012**	0.034	0.839	0.149	0.217
RBT vs. POD	**0.360**	**0.050**	0.111	0.512	0.143	0.237
%CV vs. POD	**0.760**	**<0.001**	**0.802**	**<0.001**	**0.796**	**<0.001**
All therocephalians, independent contrasts						
ln midshaft area vs. RBT	−0.466	0.174	−0.476	0.232	--	--
ln midshaft area vs. %CV	**0.765**	**0.006**	**0.807**	**0.015**	--	--
ln midshaft area vs. POD	**0.656**	**0.028**	**0.859**	**0.006**	--	--
RBT vs. %CV	−0.077	0.831	−0.224	0.592	--	--
RBT vs. POD	−0.472	0.168	−0.010	0.979	--	--
%CV vs. POD	**0.639**	**0.034**	**0.877**	**0.004**	--	--

**r and p*-values in boldface are significant at α = 0.05

PeerJ Reviewing Manuscript

Figure 1. Stratigraphic ranges of therocephalians sampled histologically in the present study. Dashed line indicates position of Permian-Triassic Boundary (PTB). Abbreviations: Chx, Changxingian; *Cisteceph* AZ, *Cistecephalus* Assemblage Zone; *Cyn* sub A, *Cynognathus* subzone A; *Eodicyno* AZ, *Eodicynodon* Assemblage Zone; Ind, Induan; Olen, Olenekian; *Pristerog* AZ, *Pristerognathus* Assemblage Zone; Roa, Roadian; *Tapinoceph* AZ, *Tapinocephalus* Assemblage Zone; *Tropido* AZ, *Tropidostoma* Assemblage Zone; Wor, Wordian. [intended for one column's width]

Figure 2. Bone histology in *Lycosuchus vanderrieti* from the Middle Permian *Tapinocephalus* Assemblage Zone. **A**, SAM-PK-9084, radius midshaft, cortical fibrolamellar bone viewed at high magnification (crossed-nicols with wave plate). **B**, Same as 'A,' viewed under normal polarized light without wave plate. **C**, SAM-PK-9084, ulna midshaft, cortex showing growth marks and well-vascularized fibrolamellar bone viewed at low magnification (non-polarized light). Note the thick bone wall and inner coarse cancellous structure. **D**, SAM-PK-K9012, femur midshaft, dorsal cortex showing subplexiform fibrolamellar bone viewed under non-polarized light. **E**, SAM-PK-K9012, femur midshaft, posterior region of cortex showing three bands of parallel-fibered bone (blue bands denoted by arrows) representing possible growth marks, viewed at low magnification (crossed-nicols with wave plate). Arrows denote growth marks. Abbreviations: po, primary osteon. [intended for two column's width]

PeerJ Reviewing Manuscript

PeerJ Reviewing Manuscript

Figure 3. Bone histology in Scylacosauridae from the Middle Permian *Tapinocephalus* Assemblage Zone. **A**, *Glanosuchus macrops*, BP/1/6228, ulna midshaft, cortical fibrolamellar bone viewed at low magnification (crossed-nicols with wave plate). **B**, Scylacosauridae indet., SAM-PK-5018, fibula midshaft close-up of secondary osteon in deep cortex (crossed-nicols with wave plate). **C**, Scylacosauridae indet., CGS R300, humerus midshaft cortex viewed at low magnification showing growth marks (crossed-nicols with wave plate). **D**, Scylacosauridae indet., BP/1/5576, ulna midshaft cortex viewed at low magnification showing growth marks (crossed-nicols with wave plate). **E**, Scylacosauridae indet., BP/1/5587, ulna midshaft cortex viewed at low magnification showing growth marks (crossed-nicols with wave plate). Arrows denote growth marks. Abbreviations: cl, cement line; Hc, Haversian canal; po, primary osteon. [intended for two column's width]

Figure 4. Bone histology in the akidnognathid *Olivierosuchus parringtoni* from the Triassic *Lystrosaurus* Assemblage Zone. **A**, NMQR 3605, cross-sectional profile of humerus midshaft viewed at low magnification (crossed-nicols with wave plate). Note the occluded medullary region and relatively thick cortical bone wall. **B**, NMQR 3605, humerus midshaft, cortical fibrolamellar bone showing large primary osteons preceding a thin zone of parallel-fibered bone near a LAG (crossed-nicols with wave plate). **C**, NMQR 3605, humerus midshaft, cortex showing thick zone of reticular fibrolamellar bone followed by parallel-fibered bone and a LAG (crossed-nicols with wave plate). **D**, Triassic *Moschorhinus* (SAM-PK-K118) humerus midshaft shown at same scale as 'C' for comparison (crossed-nicols with wave plate). Note the densely packed reticular and radial primary osteons and globular osteocyte lacunae. **E**, SAM-PK-K10617, femur midshaft, cortical fibrolamellar bone viewed at low magnification (crossed-nicols with wave plate). **F**, SAM-PK-K10617, femur midshaft, close-up of primary osteons and interstitial bone matrix (normal polarized light at maximum extinction). Arrows denote growth marks. Abbreviations: pfb, parallel-fibered bone; po, primary osteon. [intended for two column's width]

Figure 5. Bone histology in the hofmeyriid *Hofmeyria atavus*. **A**, BP/1/4404, cortex of humerus midshaft viewed at low magnification (crossed-nicols with wave plate). **B**, BP/1/4404, cross-sectional profile of radius midshaft viewed at low magnification (crossed-nicols with wave plate). **C**, Same as 'B,' close-up of cortex showing growth marks and lamellar bone in outer cortex (crossed-nicols with wave plate). **D**, Same as 'B,' close-up of cortex showing longitudinal primary osteons and outer lamellar bone (crossed-nicols with wave plate). **E**, BP/1/4404, ulna midshaft cross-section viewed at low magnification (crossed-nicols with wave plate). **F**, BP/1/4404, ulna midshaft cortex viewed at high magnification, showing sharp transition to lamellar bone in outer cortex (crossed-nicols with wave plate). Brackets denote outer zone of lamellar bone with simple canals, indicating marked decrease in bone apposition. Abbreviations: pfb, parallel-fibered bone; po, primary osteon. [intended for two column's width]

Figure 6. Bone histology in the hofmeyriid *Mirotenthes digitipes*. **A**, SAM-PK-K6511, humerus midshaft cross-section viewed at low magnification (crossed-nicols with wave plate). **B**, SAM-PK-K6511, radius midshaft cortex (crossed-nicols with wave plate). **C**, SAM-PK-K6511, ulna midshaft cortex (crossed-nicols with wave plate). **D**, SAM-PK-K6511, femur midshaft cortex showing extensive parallel-fibered and lamellar bone (normal polarized light at maximum extinction). **E**, SAM-PK-K6511, tibia midshaft cross-section viewed at low magnification (non-polarized light). **F**, SAM-PK-K6511, fibula midshaft cross-section viewed at low magnification (non-polarized light). Bracket indicates avascular outer zone. Abbreviations: pfb, parallel-fibered bone; po, primary osteon. [intended for two column's width]

Figure 7. Bone histology in the whaitsiid *Theriognathus microps*. **A**, NMQR 3375, femur midshaft cross-section viewed at low magnification (non-polarized light). **B**, NMQR 3375, femur midshaft cortical bone viewed at medium magnification showing growth marks (arrows) (non-polarized light). **C**, same as 'B,' viewed at high magnification with wave plate, showing close-up of outer zone of well-vascularized fibrolamellar bone (bracket). **D**, BP/1/719, femur midshaft cortex (crossed-nicols with wave plate). Arrows denote growth marks. Abbreviations: flb, fibrolamellar bone; rc, radial canals. [intended for two column's width]

PeerJ Reviewing Manuscript

PeerJ Reviewing Manuscript

Figure 8. Bone histology in the baurioid *Ictidosuchoides longiceps*. **A**, SAM-PK-K8659, humerus midshaft cross-section viewed at low magnification (normal polarized light). **B**, SAM-PK-K8659, radius midshaft cortex and inner cancellous bony scaffold (crossed-nicols with wave plate). **C**, SAM-PK-K8659, tibia midshaft cortex and inner cancellous bony scaffold (crossed-nicols with wave plate). **D**, SAM-PK-K8659, femur midshaft showing inner cancellous bone and outer bone compacta with a woven-fibered matrix (crossed-nicols with wave plate). **E**, SAM-PK-K10423, femur distal shaft cortex (crossed-nicols with wave plate). **F**, SAM-PK-K10423, fibula proximal shaft cortex (crossed-nicols with wave plate). **G**, BP/1/75, humerus midshaft cortex (crossed-nicols with wave plate). **H**, BP/1/4092, midshaft cross-section of large humerus viewed at low magnification (crossed-nicols with wave plate). **I**, BP/1/4092, radius close-up showing growth mark (annulus) in outer cortex (non-polarized light). Arrows denote growth marks. Abbreviations: nc, nutrient canal; pfb, parallel-fibered bone; spc, subplexiform canals; wb, woven-fibered bone. [intended for two column's width]

Figure 9. Bone histology in the baurioid *Tetracynodon darti*. **A**, NMQR 3745, humerus midshaft cross-sectional profile viewed at low magnification (non-polarized light). **B**, UCMP 78396, humerus midshaft cortex (normal polarized light at maximum extinction). Bracket denotes outer zone of parallel-fibered and lamellar bone. **C**, UCMP 78396, humerus midshaft cortex showing outer line of arrested growth (demarcated by cement line at arrow) (non-polarized light). **D**, UCMP 78395, radius midshaft cortex and perimedullary region viewed at low magnification (crossed-nicols with wave plate). **E**, UCMP 78396, femur midshaft cortex and perimedullary region showing woven- and parallel-fibered bone (crossed-nicols with wave plate). **F**, UCMP 78396, femur midshaft cortex close-up (normal polarized light at maximum extinction). **G**, UCMP 78396, fibula midshaft cortical bone packed with longitudinal primary osteons (non-polarized light). Arrows denote growth marks. Abbreviations: elb, endosteal lamellar bone; pfb, parallel-fibered bone; po, primary osteon; Sf, Sharpey's fibers; wb, woven-fibered bone. [intended for two column's width]

Figure 10. Bone histology in the baurioid *Scaloposaurus constrictus*. **A**, Humerus midshaft cross-section showing fibrolamellar bone deposition followed by a thin collar of lamellar bone in the subperiosteal region (normal polarized light at maximum extinction). **B**, Humerus midshaft cortex close-up showing longitudinal primary osteons and a large nutrient canal within a woven-fibered bone matrix (crossed-nicols with wave plate). Abbreviations: lb, lamellar bone; nc, nutrient canal; po, primary osteon. [intended for one column's width]

Figure 11. Bone histology in the baurioid *Microgomphodon oligocynus*. **A**, NMQR 3605, humerus midshaft cross-section viewed at low magnification (crossed-nicols with wave plate). Note local histovariation in the arrangements of vascular canals. **B**, NMQR 3605, femur midshaft cross-sectional profile viewed at low magnification (crossed-nicols with wave plate). **C**, Close-up of 'B' showing abundant reticular canals in cortex and lack of growth marks. **D**, NMQR 3605, tibia midshaft cross-sectional profile viewed at low magnification (crossed-nicols with wave plate). **E**, NMQR 3605, fibula midshaft cortex (crossed-nicols with wave plate). Abbreviations: cc, circular canal; rc, reticular canal; po, primary osteon; Sf, Sharpey's fibers. [intended for two column's width]

Figure 12. Linear regression of vascular growth proxies against size (midshaft cross-sectional area) from limb bone elements. **A**, Mean cortical vascularity (%*CV*) against midshaft cross-sectional area. **B**, Mean primary osteon diameter (*POD*) against midshaft cross-sectional area. **C**, mean %*CV* against mean *POD*. All correlations between vascular growth proxies and size are strongly positively correlated for both propodials (solid regression line) and epipodials (dashed regression line). Blue circles = propodials. Red circles = epipodials. [intended for one column's width]

Figure 13. Comparison of bone histology and microvasculature in Permian *Theriognathus* and *Moschorhinus*. **A**, *Theriognathus* (NMQR 3375) femur midshaft cortex (non-polarized light). **B**, *Moschorhinus* (NMQR 3939) humerus midshaft cortex (non-polarized light). Note the greater overall degree of vascularity in 'B.' [intended for two column's width]

PeerJ Reviewing Manuscript

Figure 14. Mirror phylogenies of Permo-Triassic therocephalians sampled for bone histology (scaled to geologic time). Phylogenetic character mapping of histological traits estimated from propodials (left) and epidpodials (right) reveals comparable ancestor-descendant changes for each pool of skeletal elements. **A**, average cortical vascularity (%*CV*). **B**, average primary osteon diameter (*POD*). **C**, relative bone wall thickness (*RBT*). Ancestral states were reconstructed using squared-change parsimony in Mesquite version 2.0 (Maddison and Maddison, 2007). [intended for 1.5 column's width]

PeerJ Reviewing Manuscript

Figure 1

Stratigraphic ranges of therocephalians sampled histologically in the present study.

Figure 1. Stratigraphic ranges of therocephalians sampled histologically in the present study. Dashed line indicates position of Permian-Triassic Boundary (PTB). Abbreviations: Chx, Changxingian; *Cisteceph* AZ, *Cistecephalus* Assemblage Zone; *Cyn* sub A, *Cynognathus* subzone A; *Eodicyno* AZ, *Eodicynodon* Assemblage Zone; Ind, Induan; Olen, Olenekian; *Pristerog* AZ, *Pristerognathus* Assemblage Zone; Roa, Roadian; *Tapinoceph* AZ, *Tapinocephalus* Assemblage Zone; *Tropido* AZ, *Tropidostoma* Assemblage Zone; Wor, Wordian.

PeerJ Reviewing Manuscript

PeerJ reviewing PDF | (v2013:11:1021:0:0:NEW 22 Nov 2013)

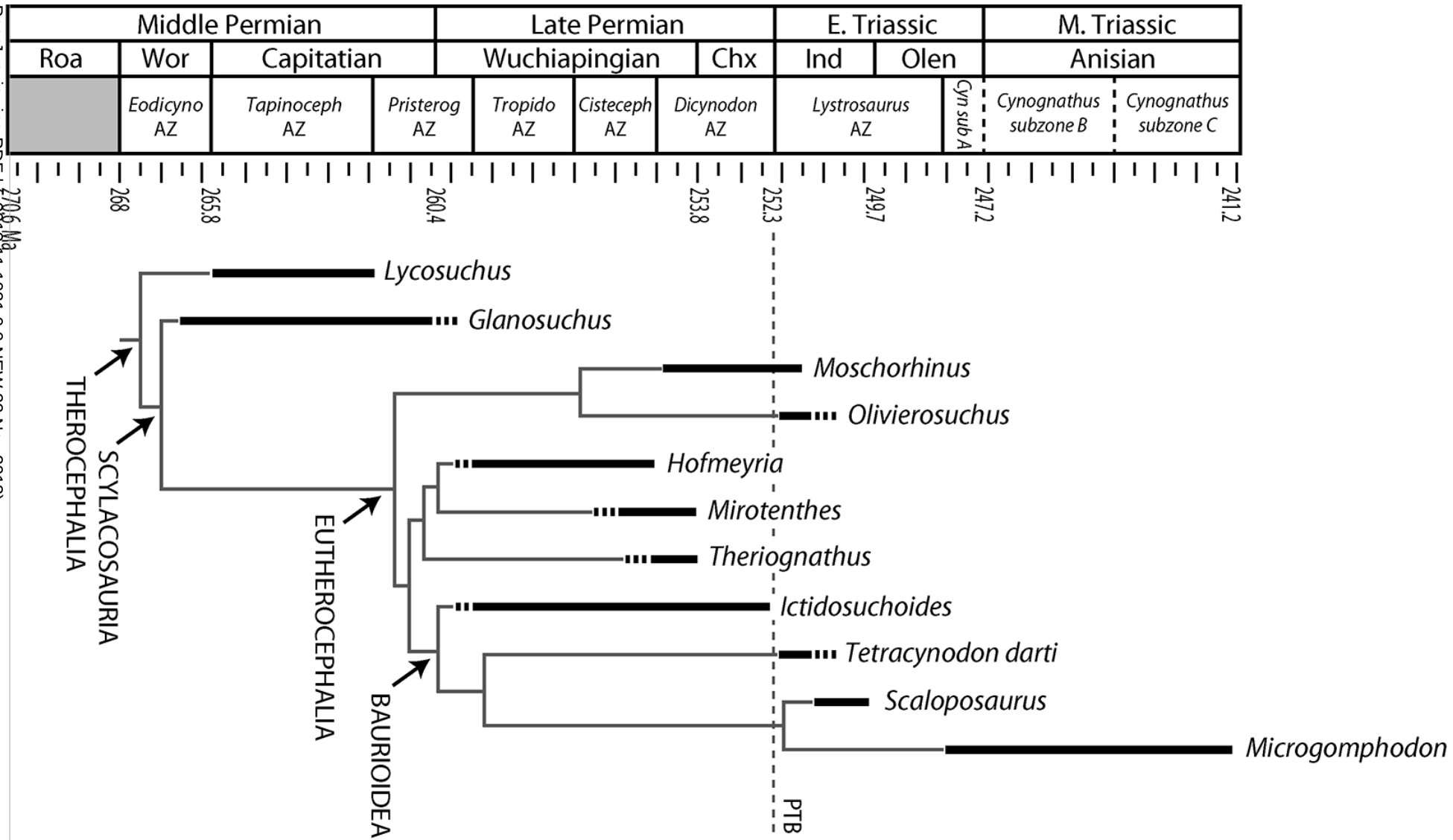

Figure 2

Bone histology in *Lycosuchus vanderrieti* from the Middle Permian *Tapinocephalus* Assemblage Zone.

Figure 2. Bone histology in *Lycosuchus vanderrieti* from the Middle Permian *Tapinocephalus* Assemblage Zone. **A**, SAM-PK-9084, radius midshaft, cortical fibrolamellar bone viewed at high magnification (crossed-nicols with wave plate). **B**, Same as 'A,' viewed under normal polarized light without wave plate. **C**, SAM-PK-9084, ulna midshaft, cortex showing growth marks and well-vascularized fibrolamellar bone viewed at low magnification (non-polarized light). Note the thick bone wall and inner coarse cancellous structure. **D**, SAM-PK-K9012, femur midshaft, dorsal cortex showing subplexiform fibrolamellar bone viewed under non-polarized light. **E**, SAM-PK-K9012, femur midshaft, posterior region of cortex showing three bands of parallel-fibered bone (blue bands denoted by arrows) representing possible growth marks, viewed at low magnification (crossed-nicols with wave plate). Arrows denote growth marks. Abbreviations: po, primary osteon.

PeerJ Reviewing Manuscript

PeerJ Reviewing Manuscript

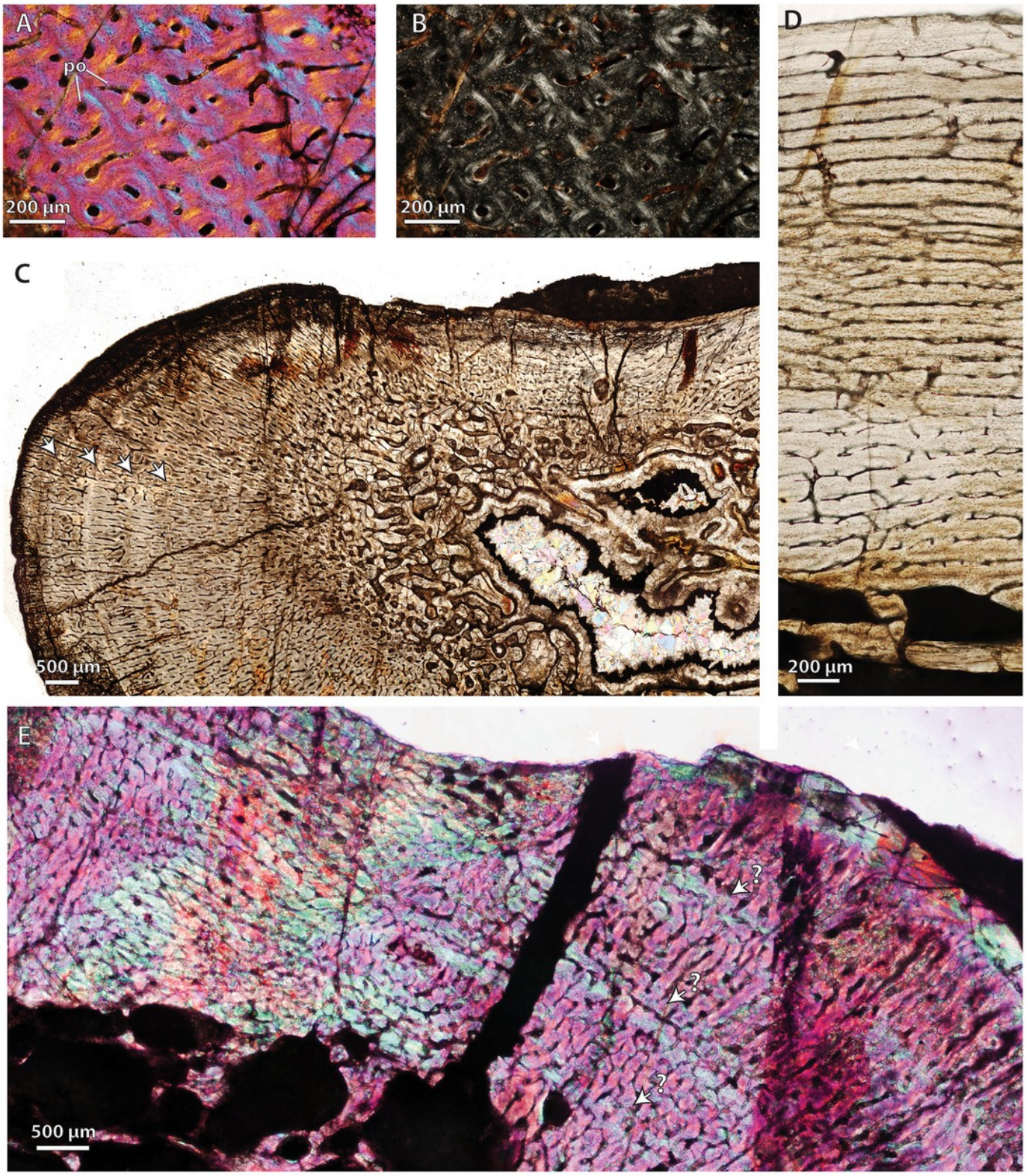

Figure 3

Bone histology in Scylacosauridae from the Middle Permian *Tapinocephalus* Assemblage Zone.

Figure 3. Bone histology in Scylacosauridae from the Middle Permian *Tapinocephalus* Assemblage Zone. **A**, *Glanosuchus macrops*, BP/1/6228, ulna midshaft, cortical fibrolamellar bone viewed at low magnification (crossed-nicols with wave plate). **B**, Scylacosauridae indet., SAM-PK-5018, fibula midshaft close-up of secondary osteon in deep cortex (crossed-nicols with wave plate). **C**, Scylacosauridae indet., CGS R300, humerus midshaft cortex viewed at low magnification showing growth marks (crossed-nicols with wave plate). **D**, Scylacosauridae indet., BP/1/5576, ulna midshaft cortex viewed at low magnification showing growth marks (crossed-nicols with wave plate). **E**, Scylacosauridae indet., BP/1/5587, ulna midshaft cortex viewed at low magnification showing growth marks (crossed-nicols with wave plate). Arrows denote growth marks. Abbreviations: cl, cement line; Hc, Haversian canal; po, primary osteon.

PeerJ Reviewing Manuscript

PeerJ Reviewing Manuscript

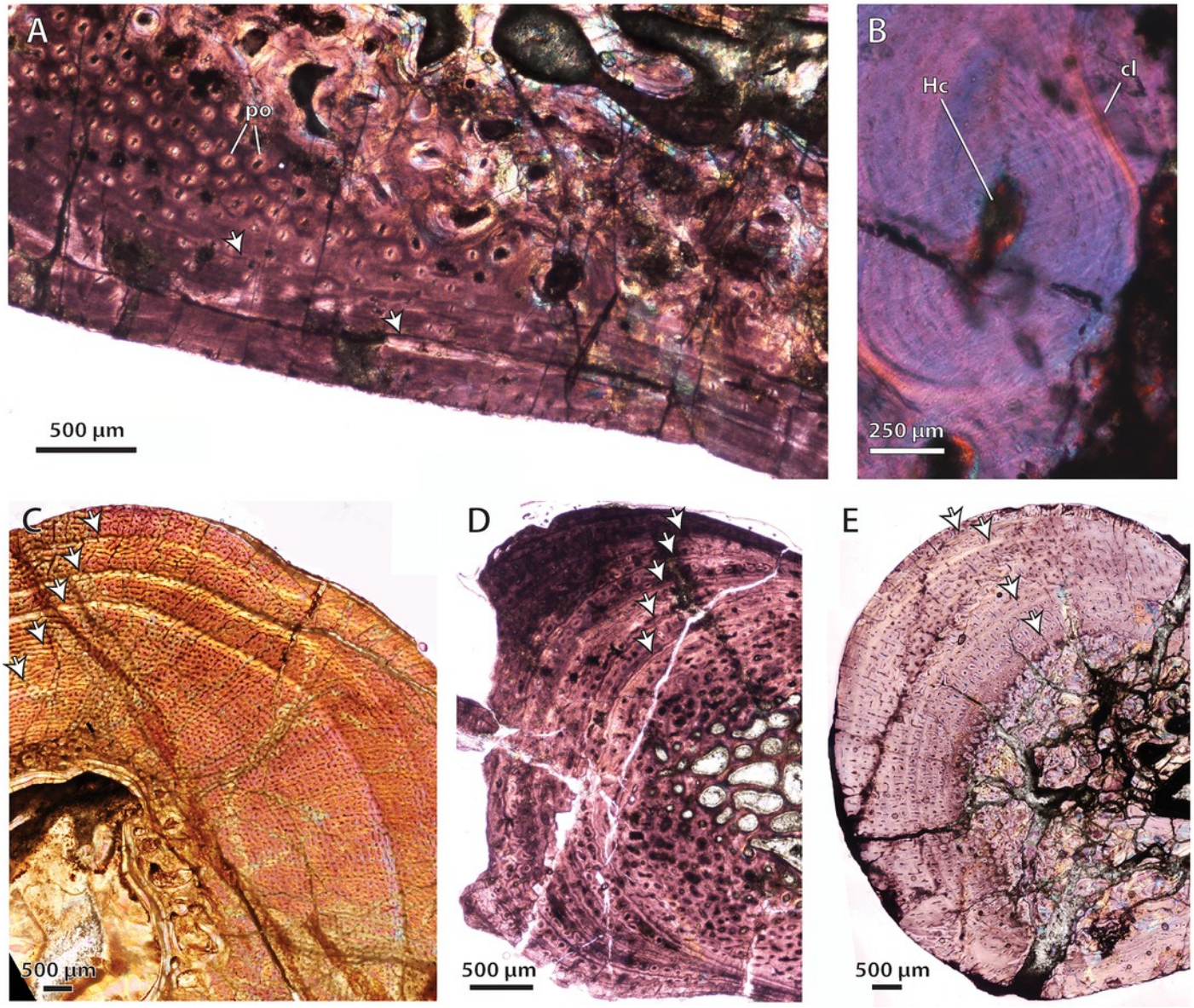

Figure 4

Bone histology in the akidnognathid *Olivierosuchus parringtoni* from the Triassic *Lystrosaurus* Assemblage Zone.

Figure 4. Bone histology in the akidnognathid *Olivierosuchus parringtoni* from the Triassic *Lystrosaurus* Assemblage Zone. **A**, NMQR 3605, cross-sectional profile of humerus midshaft viewed at low magnification (crossed-nicols with wave plate). Note the occluded medullary region and relatively thick cortical bone wall. **B**, NMQR 3605, humerus midshaft, cortical fibrolamellar bone showing large primary osteons preceding a thin zone of parallel-fibered bone near a LAG (crossed-nicols with wave plate). **C**, NMQR 3605, humerus midshaft, cortex showing thick zone of reticular fibrolamellar bone followed by parallel-fibered bone and a LAG (crossed-nicols with wave plate). **D**, Triassic *Moschorhinus* (SAM-PK-K118) humerus midshaft shown at same scale as 'C' for comparison (crossed-nicols with wave plate). Note the densely packed reticular and radial primary osteons and globular osteocyte lacunae. **E**, SAM-PK-K10617, femur midshaft, cortical fibrolamellar bone viewed at low magnification (crossed-nicols with wave plate). **F**, SAM-PK-K10617, femur midshaft, close-up of primary osteons and interstitial bone matrix (normal polarized light at maximum extinction). Arrows denote growth marks. Abbreviations: pfb, parallel-fibered bone; po, primary osteon.

PeerJ Reviewing Manuscript

PeerJ Reviewing Manuscript

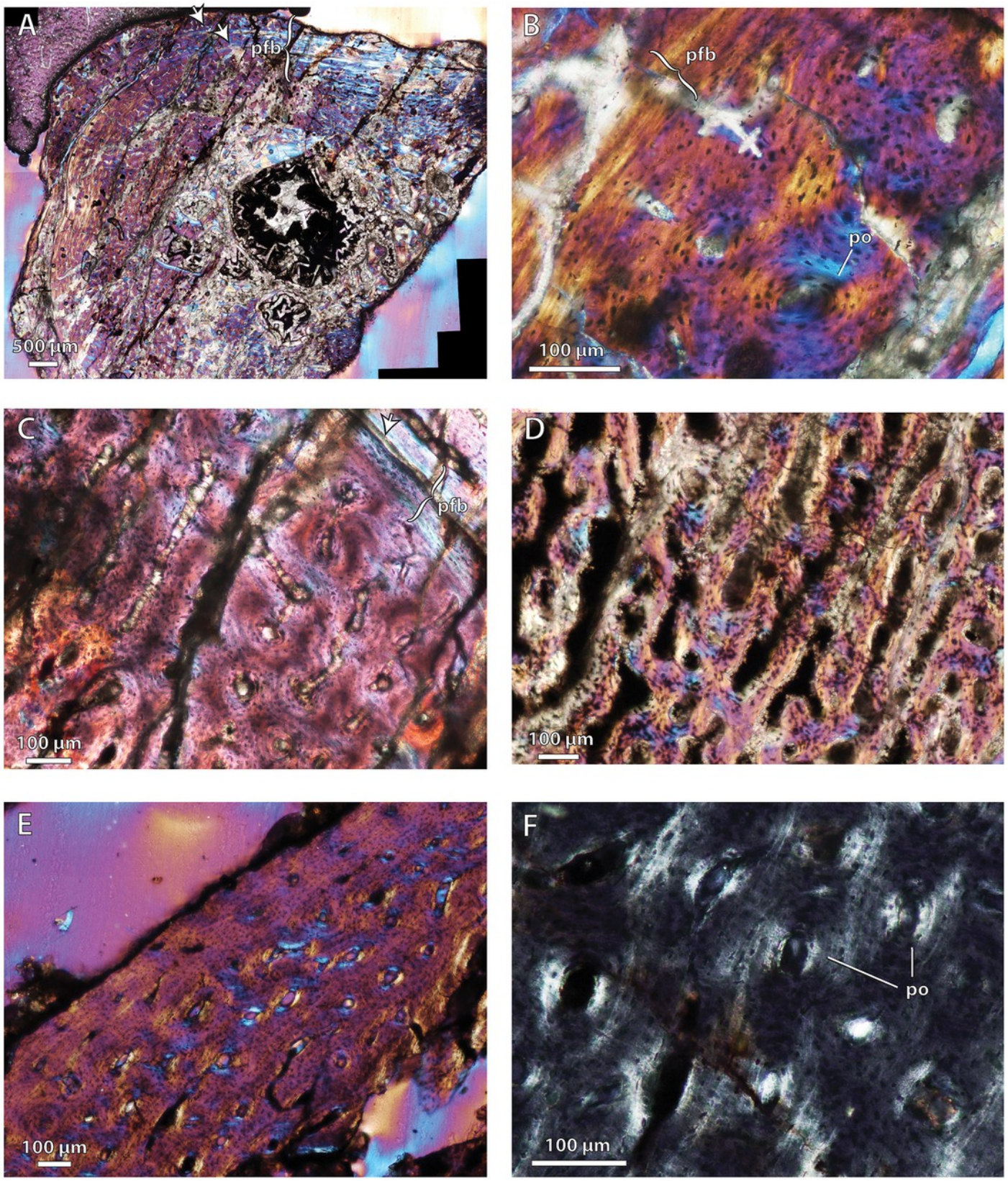

Figure 5

Bone histology in the hofmeyriid *Hofmeyria atavus*.

Figure 5. Bone histology in the hofmeyriid *Hofmeyria atavus*. **A**, BP/1/4404, cortex of humerus midshaft viewed at low magnification (crossed-nicols with wave plate). **B**, BP/1/4404, cross-sectional profile of radius midshaft viewed at low magnification (crossed-nicols with wave plate). **C**, Same as 'B,' close-up of cortex showing growth marks and lamellar bone in outer cortex (crossed-nicols with wave plate). **D**, Same as 'B,' close-up of cortex showing longitudinal primary osteons and outer lamellar bone (crossed-nicols with wave plate). **E**, BP/1/4404, ulna midshaft cross-section viewed at low magnification (crossed-nicols with wave plate). **F**, BP/1/4404, ulna midshaft cortex viewed at high magnification, showing sharp transition to lamellar bone in outer cortex (crossed-nicols with wave plate). Brackets denote outer zone of lamellar bone with simple canals, indicating marked decrease in bone apposition. Abbreviations: pfb, parallel-fibered bone; po, primary osteon.

PeerJ Reviewing Manuscript

PeerJ Reviewing Manuscript

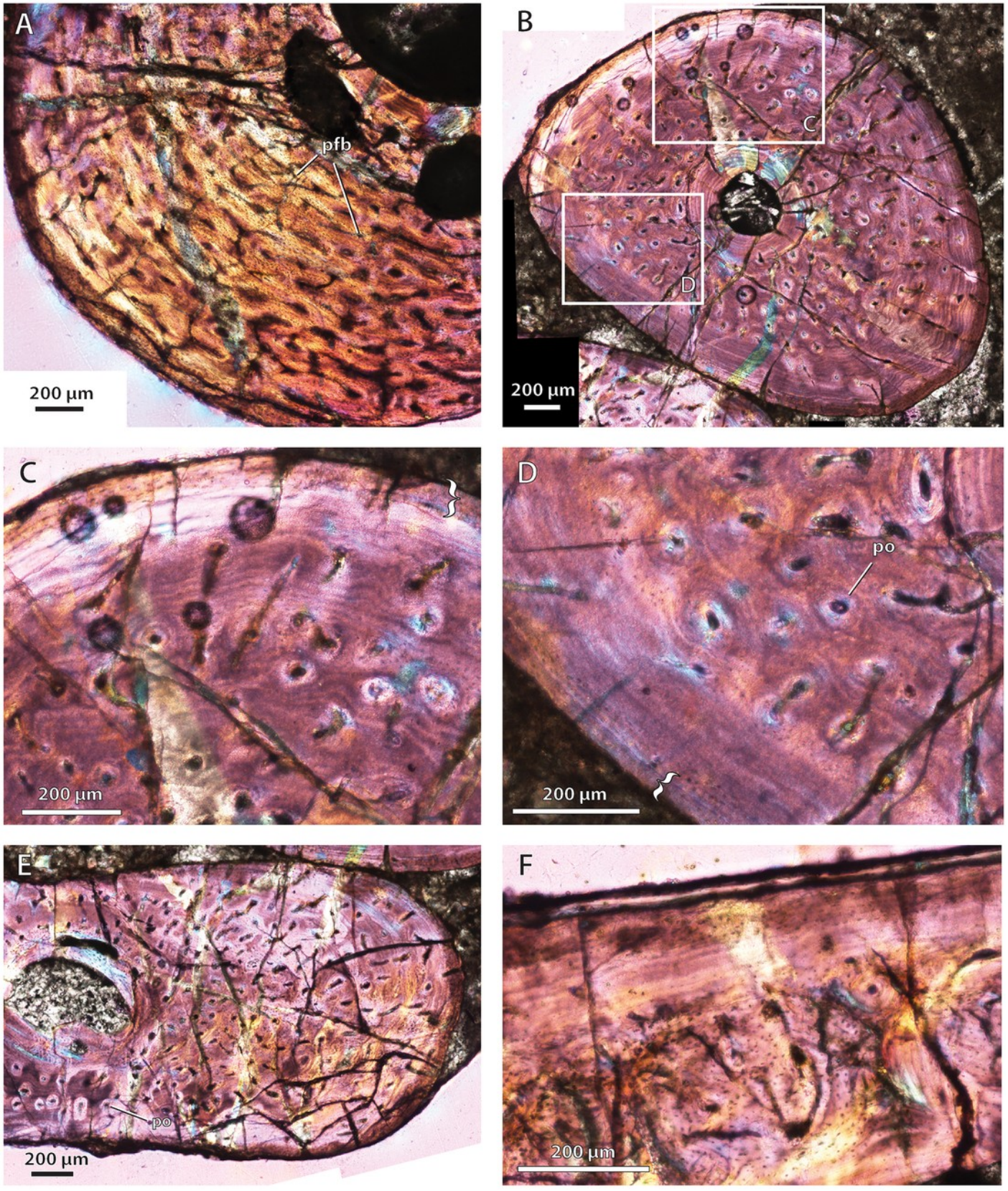

Figure 6

Bone histology in the hofmeyriid *Mirotenthes digitipes*.

Figure 6. Bone histology in the hofmeyriid *Mirotenthes digitipes*. **A**, SAM-PK-K6511, humerus midshaft cross-section viewed at low magnification (crossed-nicols with wave plate). **B**, SAM-PK-K6511, radius midshaft cortex (crossed-nicols with wave plate). **C**, SAM-PK-K6511, ulna midshaft cortex (crossed-nicols with wave plate). **D**, SAM-PK-K6511, femur midshaft cortex showing extensive parallel-fibered and lamellar bone (normal polarized light at maximum extinction). **E**, SAM-PK-K6511, tibia midshaft cross-section viewed at low magnification (non-polarized light). **F**, SAM-PK-K6511, fibula midshaft cross-section viewed at low magnification (non-polarized light). Bracket indicates avascular outer zone. Abbreviations: pfb, parallel-fibered bone; po, primary osteon.

PeerJ Reviewing Manuscript

PeerJ Reviewing Manuscript

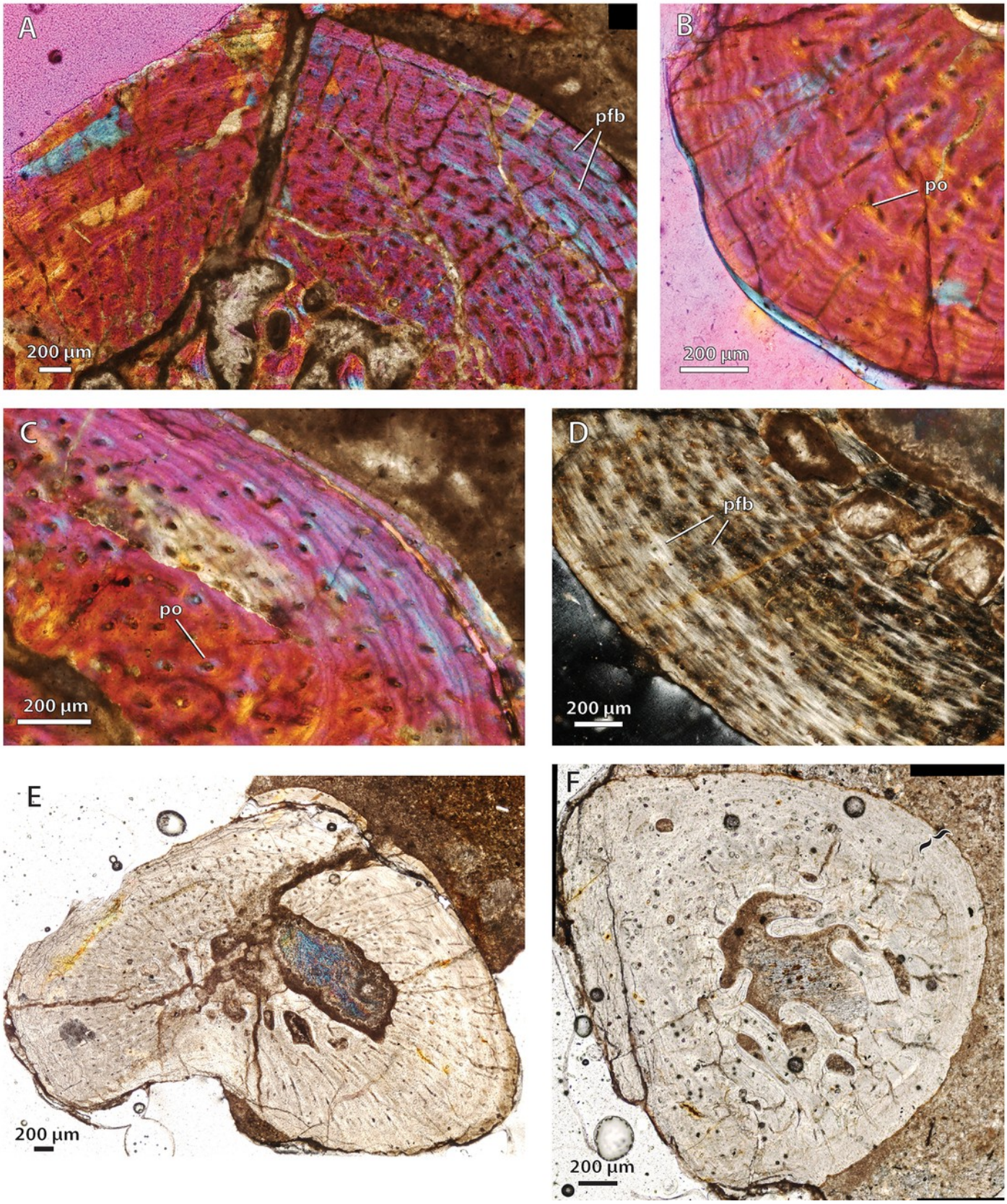

Figure 7

Bone histology in the whaitsiid *Theriognathus microps*.

Figure 7. Bone histology in the whaitsiid *Theriognathus microps*. **A**, NMQR 3375, femur midshaft cross-section viewed at low magnification (non-polarized light). **B**, NMQR 3375, femur midshaft cortical bone viewed at medium magnification showing growth marks (arrows) (non-polarized light). **C**, same as 'B,' viewed at high magnification with wave plate, showing close-up of outer zone of well-vascularized fibrolamellar bone (bracket). **D**, BP/1/719, femur midshaft cortex (crossed-nicols with wave plate). Arrows denote growth marks. Abbreviations: flb, fibrolamellar bone; rc, radial canals.

PeerJ Reviewing Manuscript

PeerJ Reviewing Manuscript

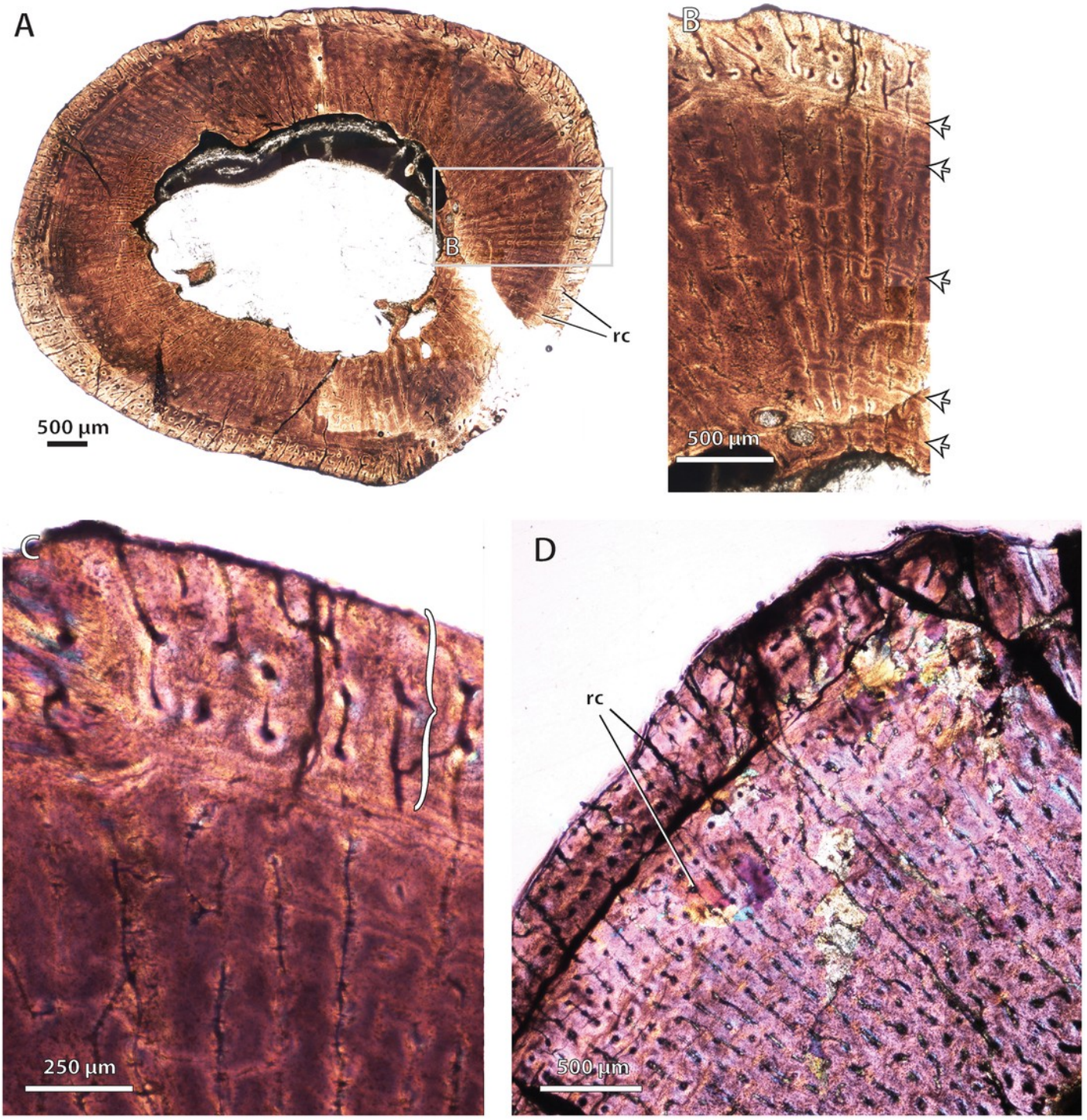

Figure 8

Bone histology in the baurioid *Ictidosuchoides longiceps*.

Figure 8. Bone histology in the baurioid *Ictidosuchoides longiceps*. **A**, SAM-PK-K8659, humerus midshaft cross-section viewed at low magnification (normal polarized light). **B**, SAM-PK-K8659, radius midshaft cortex and inner cancellous bony scaffold (crossed-nicols with wave plate). **C**, SAM-PK-K8659, tibia midshaft cortex and inner cancellous bony scaffold (crossed-nicols with wave plate). **D**, SAM-PK-K8659, femur midshaft showing inner cancellous bone and outer bone compacta with a woven-fibered matrix (crossed-nicols with wave plate). **E**, SAM-PK-K10423, femur distal shaft cortex (crossed-nicols with wave plate). **F**, SAM-PK-K10423, fibula proximal shaft cortex (crossed-nicols with wave plate). **G**, BP/1/75, humerus midshaft cortex (crossed-nicols with wave plate). **H**, BP/1/4092, midshaft cross-section of large humerus viewed at low magnification (crossed-nicols with wave plate). **I**, BP/1/4092, radius close-up showing growth mark (annulus) in outer cortex (non-polarized light). Arrows denote growth marks. Abbreviations: nc, nutrient canal; pfb, parallel-fibered bone; spc, subplexiform canals; wb, woven-fibered bone.

PeerJ Reviewing Manuscript

PeerJ Reviewing Manuscript

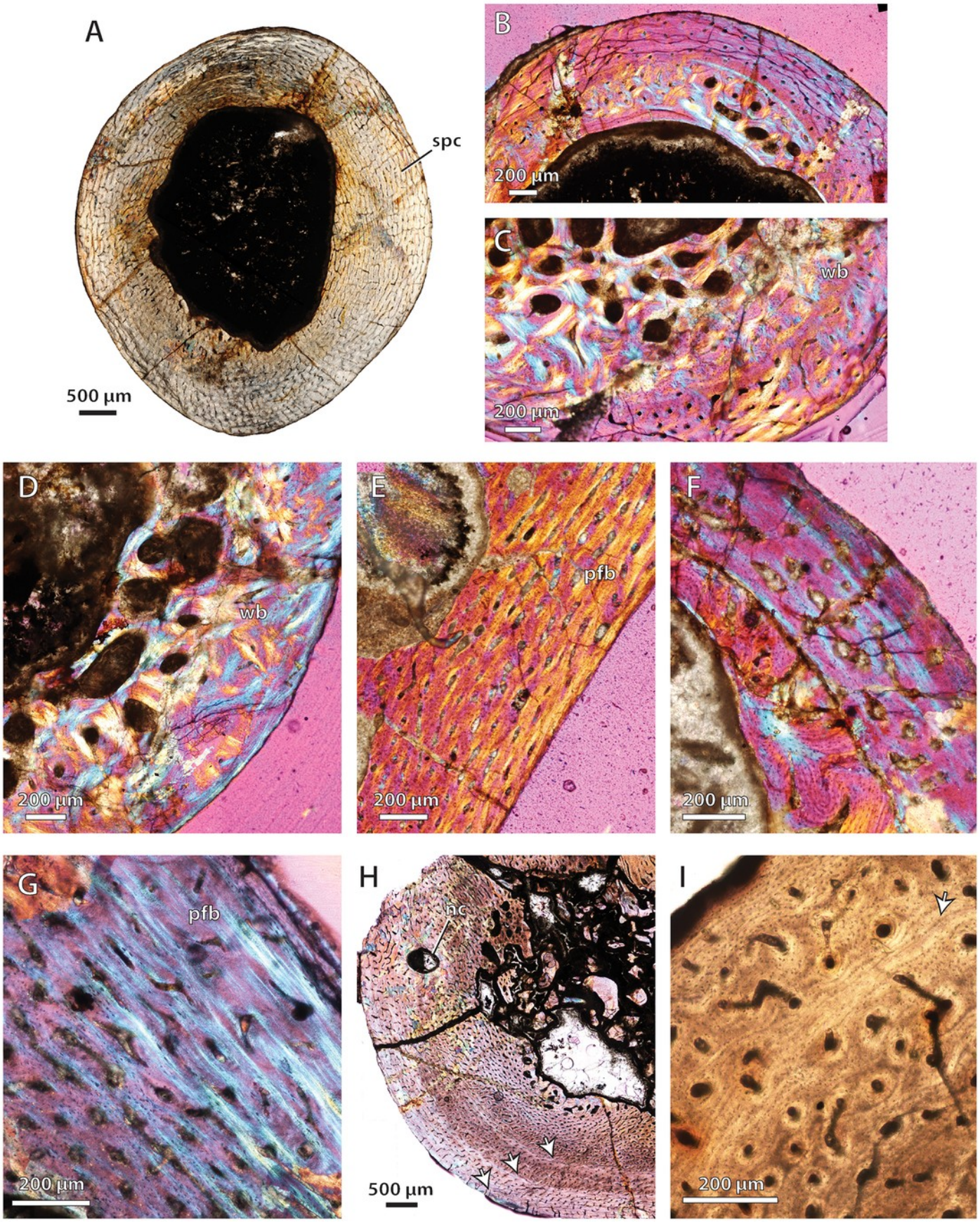

Figure 9

Bone histology in the baurioid *Tetracynodon darti*.

Figure 9. Bone histology in the baurioid *Tetracynodon darti*. **A**, NMQR 3745, humerus midshaft cross-sectional profile viewed at low magnification (non-polarized light). **B**, UCMP 78396, humerus midshaft cortex (normal polarized light at maximum extinction). Bracket denotes outer zone of parallel-fibered and lamellar bone. **C**, UCMP 78396, humerus midshaft cortex showing outer line of arrested growth (demarcated by cement line at arrow) (non-polarized light). **D**, UCMP 78395, radius midshaft cortex and perimedullary region viewed at low magnification (crossed-nicols with wave plate). **E**, UCMP 78396, femur midshaft cortex and perimedullary region showing woven- and parallel-fibered bone (crossed-nicols with wave plate). **F**, UCMP 78396, femur midshaft cortex close-up (normal polarized light at maximum extinction). **G**, UCMP 78396, fibula midshaft cortical bone packed with longitudinal primary osteons (non-polarized light). Arrows denote growth marks. Abbreviations: elb, endosteal lamellar bone; pfb, parallel-fibered bone; po, primary osteon; Sf, Sharpey's fibers; wb, woven-fibered bone.

PeerJ Reviewing Manuscript

PeerJ Reviewing Manuscript

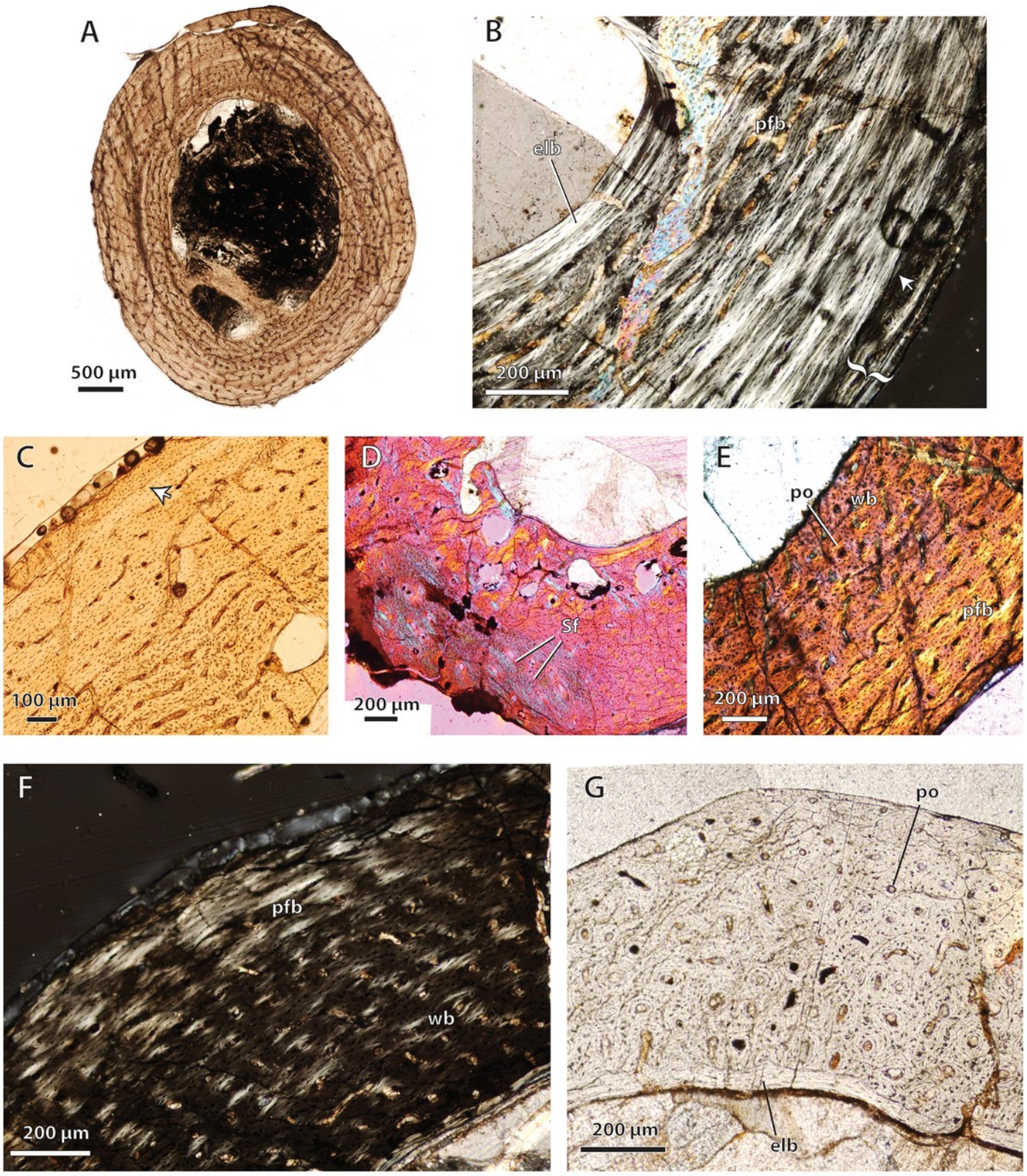

Figure 10

Bone histology in the baurioid *Scaloposaurus constrictus*.

Figure 10. Bone histology in the baurioid *Scaloposaurus constrictus*. **A**, Humerus midshaft cross-section showing fibrolamellar bone deposition followed by a thin collar of lamellar bone in the subperiosteal region (normal polarized light at maximum extinction). **B**, Humerus midshaft cortex close-up showing longitudinal primary osteons and a large nutrient canal within a woven-fibered bone matrix (crossed-nicols with wave plate). Abbreviations: lb, lamellar bone; nc, nutrient canal; po, primary osteon.

PeerJ Reviewing Manuscript

PeerJ Reviewing Manuscript

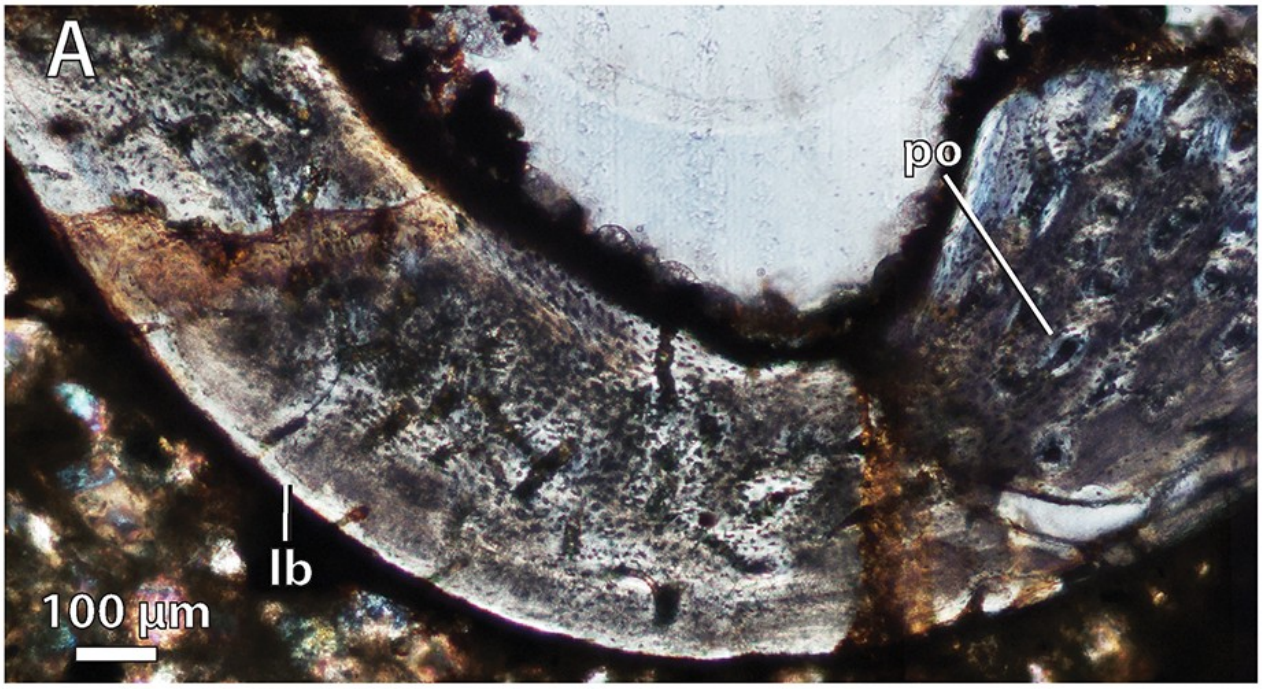

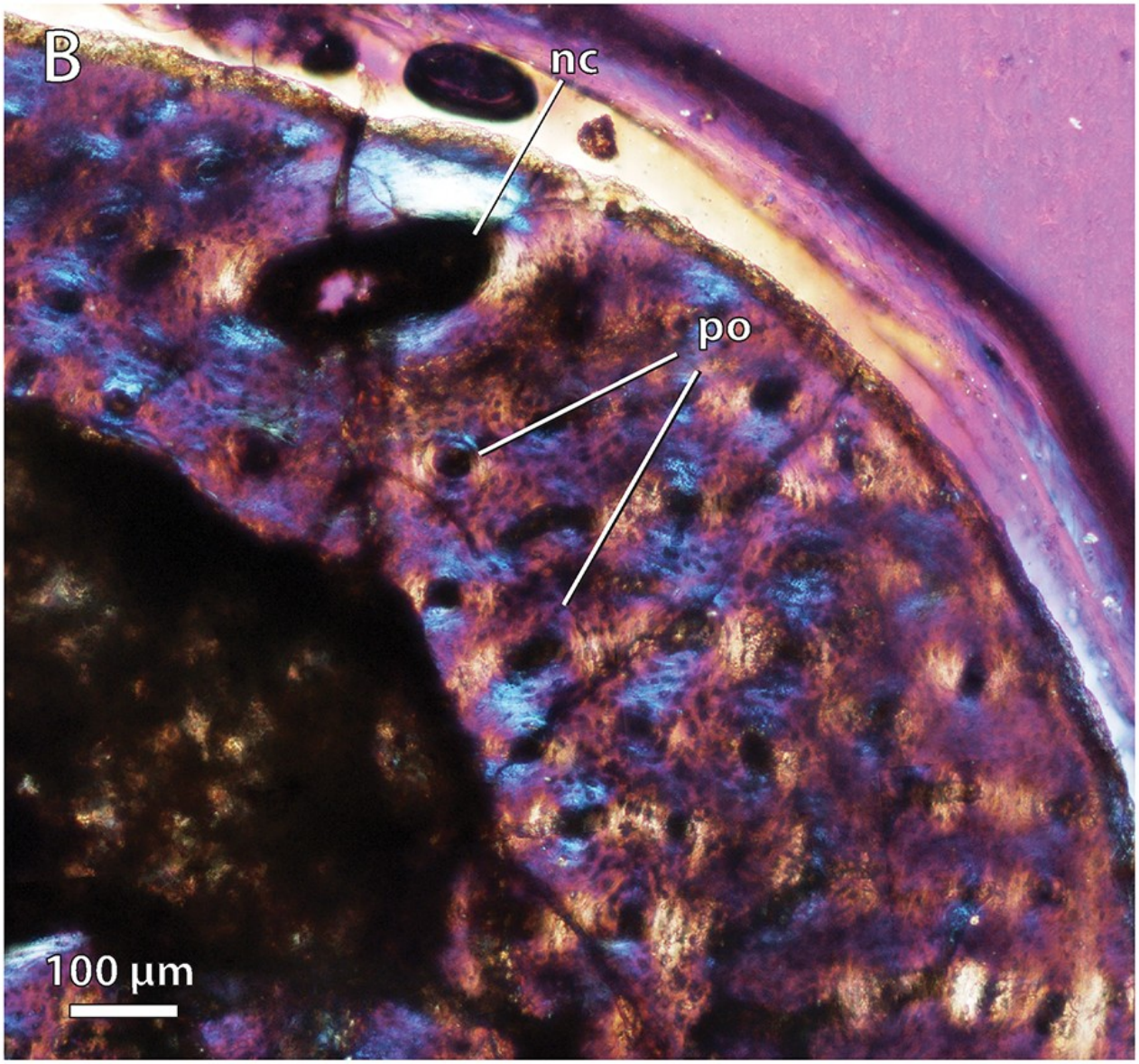

PeerJ Reviewing Manuscript

Figure 11

Bone histology in the baurioid *Microgomphodon oligocynus*.

Figure 11. Bone histology in the baurioid *Microgomphodon oligocynus*. **A**, NMQR 3605, humerus midshaft cross-section viewed at low magnification (crossed-nicols with wave plate). Note local histovariation in the arrangements of vascular canals. **B**, NMQR 3605, femur midshaft cross-sectional profile viewed at low magnification (crossed-nicols with wave plate). **C**, Close-up of 'B' showing abundant reticular canals in cortex and lack of growth marks. **D**, NMQR 3605, tibia midshaft cross-sectional profile viewed at low magnification (crossed-nicols with wave plate). **E**, NMQR 3605, fibula midshaft cortex (crossed-nicols with wave plate). Abbreviations: cc, circular canal; rc, reticular canal; po, primary osteon; Sf, Sharpey's fibers.

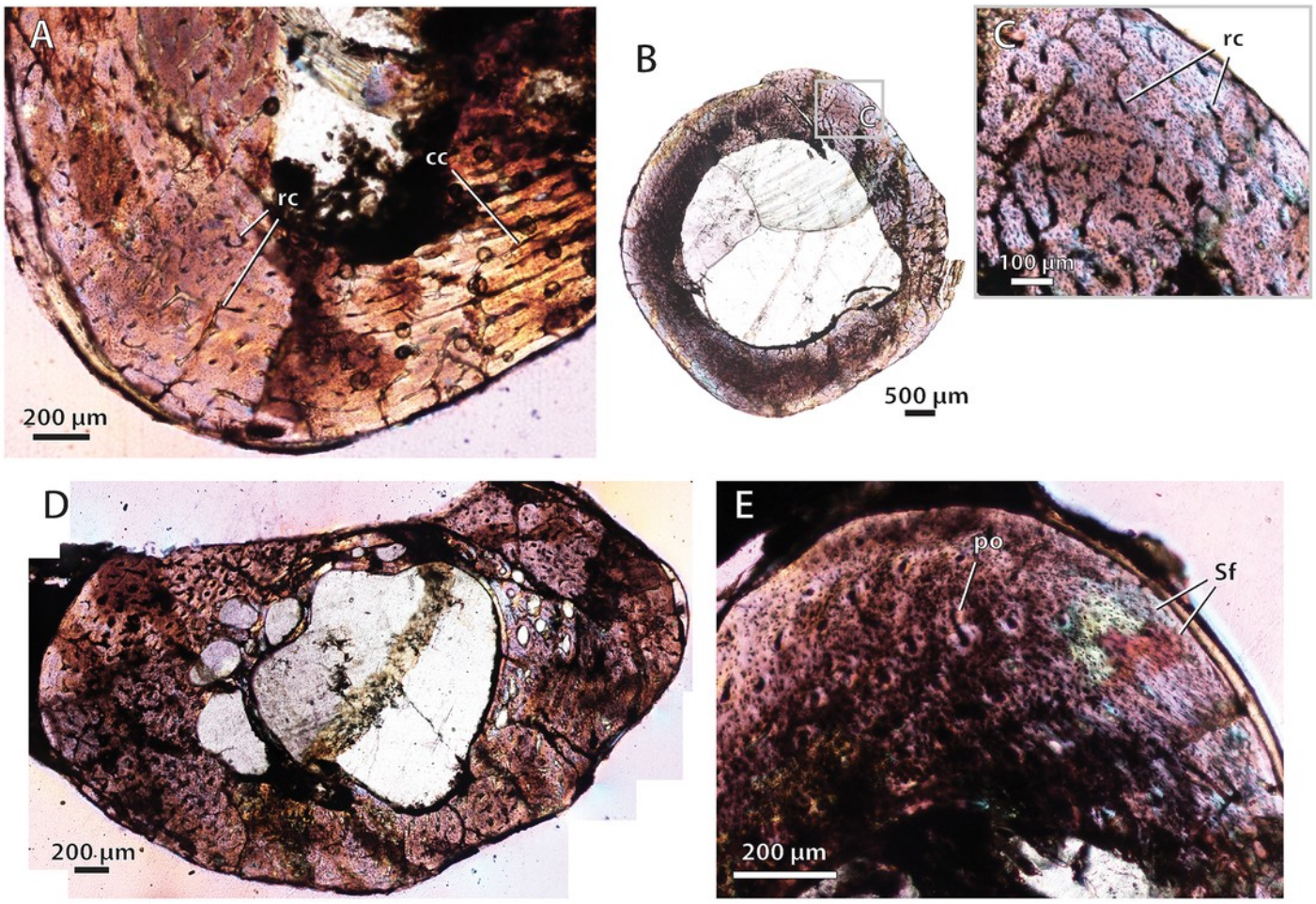

Figure 12

Linear regression of vascular growth proxies against size (midshaft cross-sectional area) from limb bone elements.

Figure 12. Linear regression of vascular growth proxies against size (midshaft cross-sectional area) from limb bone elements. **A**, Mean cortical vascularity (%*CV*) against midshaft cross-sectional area. **B**, Mean primary osteon diameter (*POD*) against midshaft cross-sectional area. **C**, mean %*CV* against mean *POD*. All correlations between vascular growth proxies and size are strongly positively correlated for both propodials (solid regression line) and epipodials (dashed regression line). Blue circles = propodials. Red circles = epipodials.

PeerJ Reviewing Manuscript

PeerJ Reviewing Manuscript

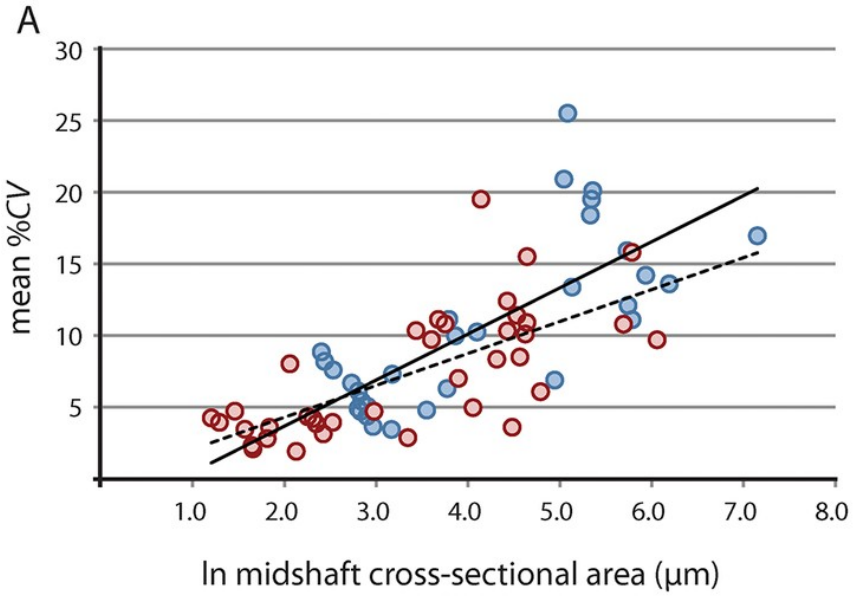

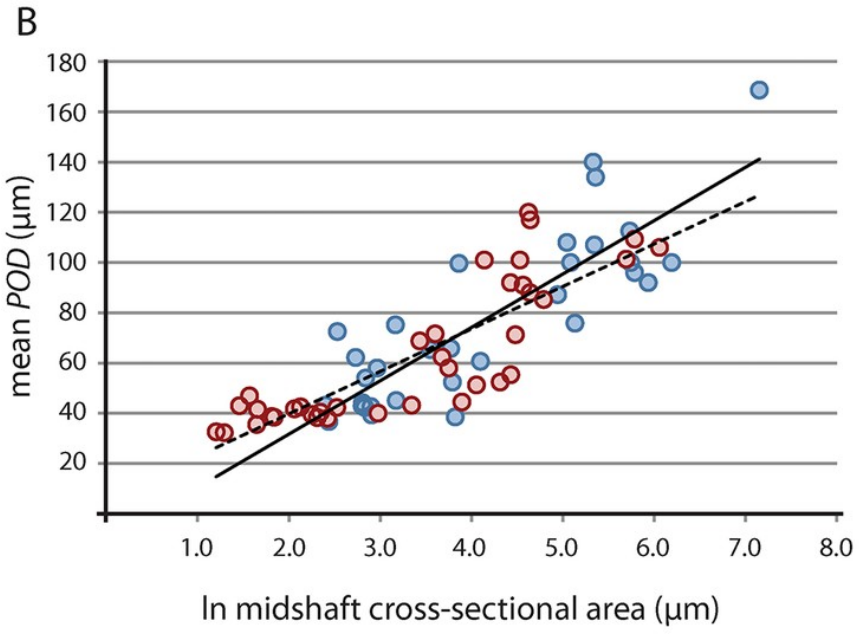

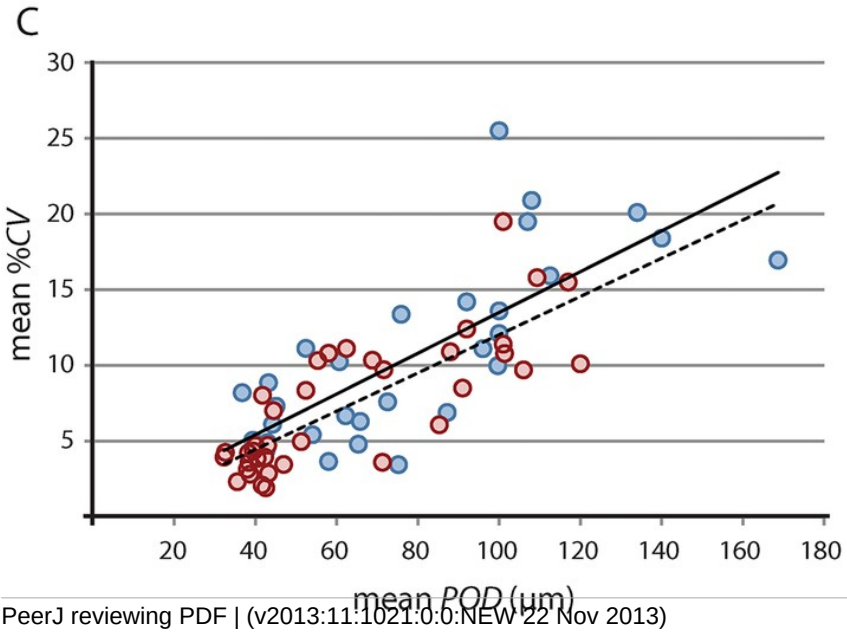

Figure 13

Comparison of bone histology and microvasculature in Permian *Theriognathus* and *Moschorhinus*.

Figure 13. Comparison of bone histology and microvasculature in Permian *Theriognathus* and *Moschorhinus*. **A**, *Theriognathus* (NMQR 3375) femur midshaft cortex (non-polarized light). **B**, *Moschorhinus* (NMQR 3939) humerus midshaft cortex (non-polarized light). Note the greater overall degree of vascularity in 'B.'

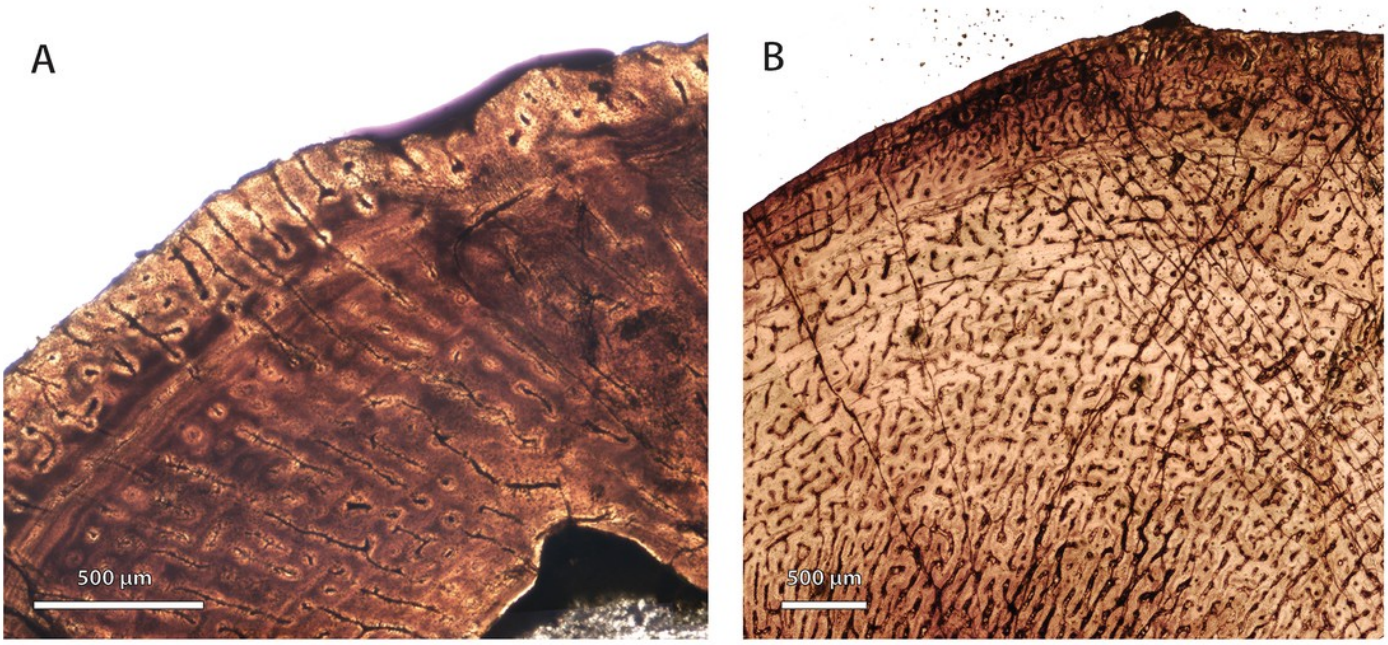

PeerJ Reviewing Manuscript

Figure 14

Mirror phylogenies of Permo-Triassic therocephalians sampled for bone histology (scaled to geologic time).

Figure 14. Mirror phylogenies of Permo-Triassic therocephalians sampled for bone histology (scaled to geologic time). Phylogenetic character mapping of histological traits estimated from propodials (left) and epidpodials (right) reveals comparable ancestor-descendant changes for each pool of skeletal elements. **A**, average cortical vascularity (%*CV*). **B**, average primary osteon diameter (*POD*). **C**, relative bone wall thickness (*RBT*). Ancestral states were reconstructed using squared-change parsimony in Mesquite version 2.0 (Maddison and Maddison, 2007).

PeerJ Reviewing Manuscript
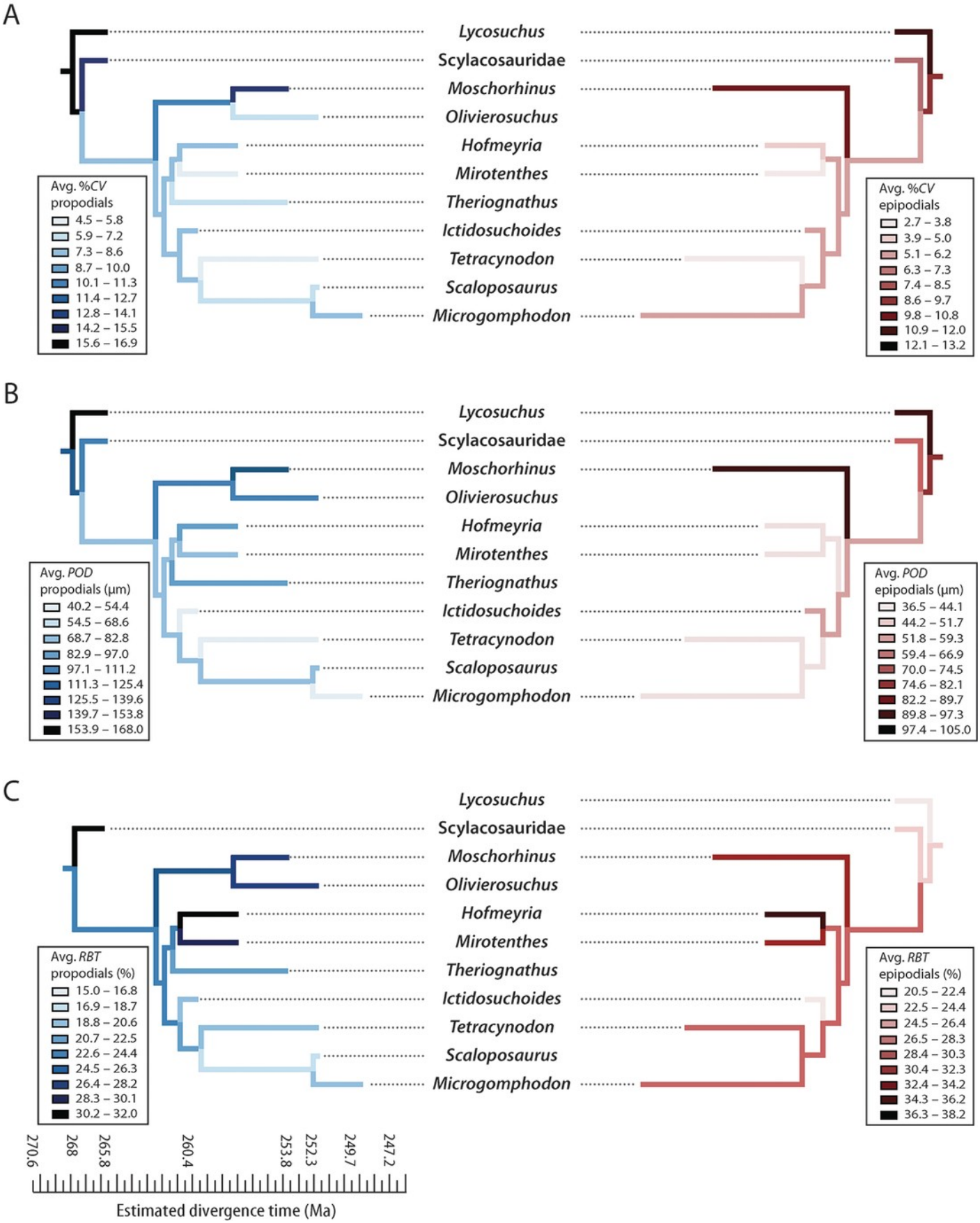
PeerJ Reviewing Manuscript